ATOMISTIC MODELLING OF ANISOTROPIC ETCHING OF CRYSTALLINE SILICON

Miguel A. Gosálvez

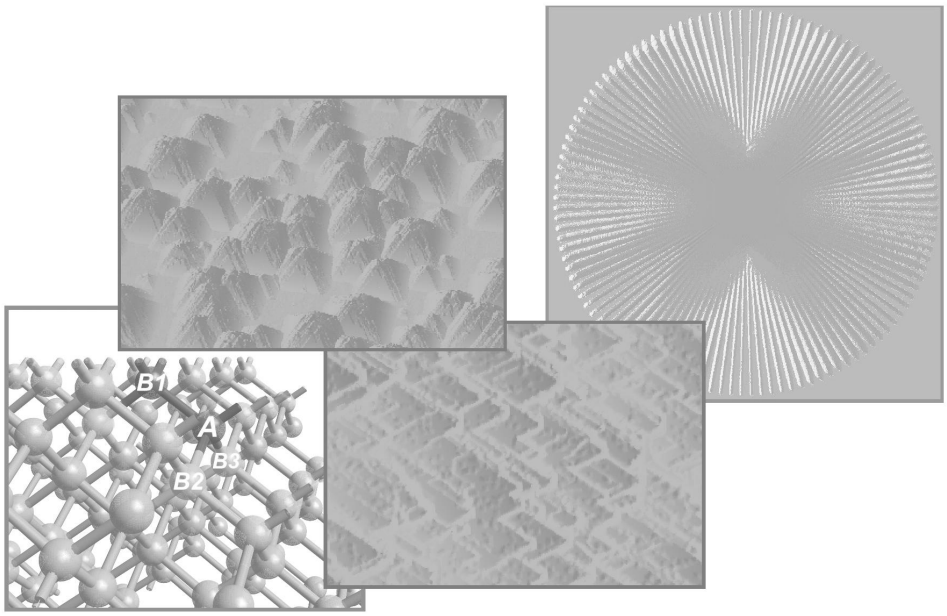

Laboratory of Physics
Helsinki University of Technology

Fysiikan laboratorio
Teknillinen korkeakoulu

DISSERTATION 123 (2003)

ATOMISTIC MODELLING OF ANISOTROPIC ETCHING OF CRYSTALLINE SILICON

Miguel A. Gosálvez

Laboratory of Physics
Helsinki University of Technology
Espoo, Finland

Dissertation for the degree of Doctor of Science in Technology to be presented with due permission of the Department of Engineering Physics and Mathematics, Helsinki University of Technology for public examination and debate in Council Room H304 at Helsinki University of Technology (Espoo, Finland) on the 19th of September, 2003, at 12 o'clock noon.

Dissertations of Laboratory of Physics, Helsinki University of Technology
ISSN 1455-1802

Dissertation 123 (2003):
Miguel A. Gosálvez: Atomistic Modelling of Anisotropic Etching of Crystalline Silicon
ISBN 951-22-6706-3 (print)
ISBN 951-22-6707-1 (electronic)

OTAMEDIA OY
ESPOO 2003

The passionate raise the world. The sceptic keep it going.

Abstract

An atomistic model for the simulation of anisotropic wet chemical etching of crystalline silicon is developed. Special attention is paid to the relation between the atomistic processes, the mesoscopic features of the surface morphology and the macroscopic anisotropy of the process, bridging the different length scales.

The development of the atomistic model is made by direct comparison of atomistic kinetic Monte Carlo and Cellular Automaton simulations with experimental results, guided by first-principles calculations. The model explains the anisotropy of the etching process and the orientation-dependent surface morphology as two different manifestations of the same atomistic mechanisms, namely, the weakening of backbonds following OH termination of surface atoms and the existence of significant interaction between the terminating species (H/OH). The versatility of the atomistic model is demonstrated by the concentration and time dependence of the simulated under-etched structures and surface morphology.

A substantial effort has been made to develop an efficient program in order to simulate the etching process in arbitrarily oriented, large, micrometer-scale systems in the presence (or absence) of masking patterns and considering the effects of temperature and etchant concentration. The program has a great potential for use in the optimization of the processing parameters in industrial applications.

Preface

This thesis has been prepared in the Laboratory of Physics at Helsinki University of Technology during the years 1998 - 2003. I want to express my most sincere gratitude to Academy Professor Risto Nieminen, my supervisor and advisor during these years. He has not only secured the necessary funding and provided excellent computational and working conditions during this period, but also offered friendly and almost inconditional moral support to my research. His vision of future, ample understanding of physics - and other dimensions of life - and his relaxed attitude make him an enjoyable interlocutor. Armed with an enourmous patience, a great dosis of trust and a flexible - but critical - open mind, he has granted almost complete freedom to carry out this thesis in the way that I have chosen and provided the necessary wise advice at the delicate moments.

I want to thank Dr. Adam Foster for being such an enjoyable chap and a great friend. In addition to the fact that this thesis would have had a much narrower perspective without his contribution, I have enjoyed chatting, practicing sports and passing the time together. My most special thanks to Dr. Andrés Ayuela for his good advice during our common time in this Laboratory and for a good solid friendship. His special interest in my work during the last months provided very fruitful, intense discussions which I will always remember warmly in my mind. Many thanks to Dr. Manuel Pérez Jigato for his extraordinary sense of humour, which has flooded pleasantly many lunch hours, and for numerous discussions and good advice in many occasions. Thanks also to Henry Pinto for a good friendship, multiple discussions and great time together. Many thanks to Dr. Young-Joo Lee for being a friend, for openly expressing his admiration for the results in this thesis and for numerous talks and advice.

I am thankful to Professor Pekka Hautojärvi for offering me repeatedly the possibility to teach in his courses and stimulating the search of major ideas when teaching other students. Special thanks to Professor Aarne Oja, who got interested in my skills in a time of economical difficulties and made it possible for me to meet Professor Risto Nieminen. Thanks to Professor Kai Nordlund for interesting observations and comments while refereeing this thesis. Thanks to Petteri Kilpinen, Eero Haimi and Professor Veikko Lindroos for fruitful collaboration and discussions. Talking with Petteri at an early stage ignited some of the ideas that have turned out crucial for the thesis.

I would like to thank my office mates Mika Heiskänen, Roberto Simola, Yihye Shim, Esa Räsänen and Ville Vuorinen for letting me feel in nice company, even though I have systematically sabotaged their ears with my musical taste. Thanks to Oskari Jääskeläinen, Sami Siljamäki and Ivan Degtyarenko for their help and advice in the use of computers. Thanks to Eija Järvinen and Helena Suvanto for many pleasant talks - and corresponding good occasions to improve my skills in Finnish -, for precious help with administrative tasks and for contributing to make me feel in a pleasant environment. Thanks in deed to all members of the Laboratory of Physics with whom I have interacted in one way or another. The list is simply just too long.

I want to thank Kari Kyhälä and Jatta-Leena Hakkarainen for a solid friendship through all these years in Finland.

My deepest emotional thanks to my mother, who has supported with painful effort but joyful interest my career through difficult family problems and disease.

My warmest thanks to Kirsi for her love, patience, inconditional support and understanding of my sometimes-obsesive way of working, and to my daughter for making me a father and for being a perfect medicine with her only presence.

Otaniemi, August 2003

Miguel A. Gosálvez

Contents

Abstract i

Preface ii

List of publications v

1 Introduction 1

2 Anisotropic wet chemical etching 3

3 Electrochemistry 7

3.1 Chemical oxidation 8

3.2 Electrochemical oxidation 10

4 Simulating anisotropic etching 12

4.1 Alternative methods 12

4.2 Atomistic model 14

4.3 Monte Carlo and Cellular Automaton simulation schemes . . 19

5 Overview of results 23

5.1 Anisotropy 23

5.2 Morphology 24

5.3 Time evolution 25

5.4 Concentration dependence 28

5.5 Temperature dependence, activation energy 31

6 Summary of Publications 34

6.1 Publication I 34

6.2 Publication II 34

6.3 Publication III 35

6.4 Publication IV 35

6.5 Publication V 36

6.6 Publication VI 36

List of publications

This Thesis consists of an overview and the following publications:

I. M. A. Gosálvez, R. M. Nieminen, P. Kilpinen, E. Haimi, and V. Lindroos, *Anisotropic Wet Chemical Etching of Crystalline Silicon: Atomistic Monte-Carlo Simulations and Experiments*, Appl. Surf. Sci. **178**, 7–26 (2001).

II. M. A. Gosálvez, A. S. Foster, and R. M. Nieminen, *Multiscale modelling of anisotropic wet chemical etching of crystalline silicon*, Europhys. Lett. **60**, 467–473 (2002).

III. M. A. Gosálvez, A. S. Foster, and R. M. Nieminen, *Atomistic simulations of surface coverage effects in anisotropic wet chemical etching of crystalline silicon*, Appl. Surf. Sci. **201**, 160–182 (2002).

IV. M. A. Gosálvez, A. S. Foster, and R. M. Nieminen, *Dependence of the Anisotropy of Wet Chemical Etching of Silicon on the Amount of Surface Coverage by OH Radicals*, Sensors and Materials **15**, 53–65 (2003).

V. M. A. Gosálvez, and R. M. Nieminen, *Surface morphology during anisotropic wet chemical etching of crystalline silicon*, New J. Phys. **5**, 100 (2003).

VI. M. A. Gosálvez, and R. M. Nieminen, *Relation between macroscopic and microscopic activation energies in non-equilibrium surface processing*, Phys. Rev. E, in press (2003).

The author has had an active role in all phases of the research reported in this Thesis. He has been involved in planning and performing the simulations, and in the interpretation of the results. He has had an important role in the conceptualization of the atomistic model presented in Publications I-V and in the derivation of the analytical results of Publication VI. He has written all the computer programs and algorithms used in the simulations, except for the First-Principles calculations in Publication III. The author has written all the Publications.

No endeavor that is worthwhile is simple in prospect; if it is right, it will be simple in retrospect.

– Edward Teller

1 Introduction

Anisotropic wet chemical etching remains the most widely used processing technique in silicon technology. As a result of the maturity reached in integrated-circuit processing, anisotropic etching is nowadays used in combination with a multitude of other processing techniques for the manufacture of a wide range of applications in Microelectromechanical Systems (MEMS) and Micro System Technology (MST). Examples of such devices include pressure [1, 2], acceleration [3], angular rate [2] and gas-flow sensors [2, 4], actuators [5], nanoprobes [6, 7], nanowires [7], micromirrors [8], laser cavities [9], optical switches [10, 11], alignment grooves [12] and microvalves [13], to mention only some. The wide presence of anisotropic etching is not only due to its ease of use and low cost, but also to the fact that it provides rather smooth surfaces with no physical damage to the bulk structure of the material. It also enables controlled undercutting of suspended structures, intractable by other microfabrication techniques. Anisotropic etching is an outstanding technique for the production of device features at the nanometer scale [14]. From a more fundamental point of view, the precision and reproducibility of the anisotropically etched surfaces serves as a model system for the study of the microscopic processes that take place at a fluid-solid interface [15].

In spite of the technological maturity in the use of anisotropic etching for applications, the complexity of the process, which involves chemical and electrochemical reactions that are sensitive to a multitude of parameters, has traditionally hindered satisfactory understanding of this technique. It is only in the last ten years that significant advances have been achieved, mainly resulting from the maturity reached in surface scanning microscopies, vibrational spectroscopies and electrochemical techniques, but also due to the availability of fast computers that have enabled large atomistic simulations of the processes. The application of surface scanning probes such as Scanning Tunneling Microscopy (STM) [15, 16, 17, 18, 19], Scanning Electron Microscopy (SEM) [12, 20, 21, 22, 23] and Atomic Force Microscopy (AFM) [24, 25, 26], has enabled an unprecedented description of the surface roughness and morphology at and below the micrometer scale, allowing the analysis of the mechanisms of nucleation, growth and evolution of surface defects such as pits, islands, hillocks and steps. By comparison with computational simulations [27, 28], these techniques have provided an invaluable source of information on the essential atomistic pro-

cesses. The use of spectroscopic techniques such as X-ray Photoelectron Spectroscopy (XPS) [21, 29, 30], InfraRed Absorption Spectroscopy (IRAS) [31, 32, 33, 34, 35, 36, 37] and Raman spectroscopy [38, 39] has provided information on the specific nature of the surface terminating species, complementing the lack of chemical sensitivity of the scanning microscopies. Electrochemical studies [17, 21, 40, 41, 42, 43] have provided important information on the complicated chemical and electrochemical nature of the reactions, thus revealing the double personality of anisotropic etching. The use of atomistic simulations [44, 45, 46] has uncovered the existence of deep relations between the different length scales, showing that the orientation dependence of the macroscopic etching process and the microscopic details of the surface morphology are different manifestations of the same atomistic processes (Publications I - V). As a result of this experimental and computational advancement, an important change of mentality has progressively taken place. Anisotropic etching is not considered any more as a macroscopic process involving the optimization of an evolving facetted surface, but rather, as a manifestly non-equilibrium process dominated by atomistic mechanisms leading to corrugated, defective surfaces.

In this Thesis, the atomistic aspects of the etching process are emphasized. A comprehensive atomistic model containing the essential ingredients for the simulation of anisotropic etching is developed, giving special attention to the relation between the atomistic processes, the mesoscopic features of the surface morphology and the macroscopic anisotropy of the process, building in this way a bridge between the different length scales. As the major content of the Thesis, Publications I-VI can be considered as a chronological evolution of the development of the model. In Publication I, the need to consider the atomistic aspects of the surface reactions in order to describe the anisotropy of the process is demonstrated. A physically meaningful way to do this is presented in Publication II, which is further completed and refined in Publication III. The two essential atomistic processes responsible for the macroscopic anisotropy are briefly described in Publication IV. By including an analysis of the mesoscopic surface morphology, Publication V shows more clearly the deep relation between the microscopic, mesoscopic and macroscopic length scales. The intimate relation between the different length scales is once again stressed in Publication VI in which an unexpected link between microscopic and macroscopic activation energies is uncovered.

2 Anisotropic wet chemical etching

When a piece of a crystalline material (such as silicon) is immersed in an alkaline or acidic solution, removal of material from the surface of the sample occurs as a result of complicated chemical reactions between the surface atoms and the etchant molecules (Fig. 1(a)). The fact that the initial shape

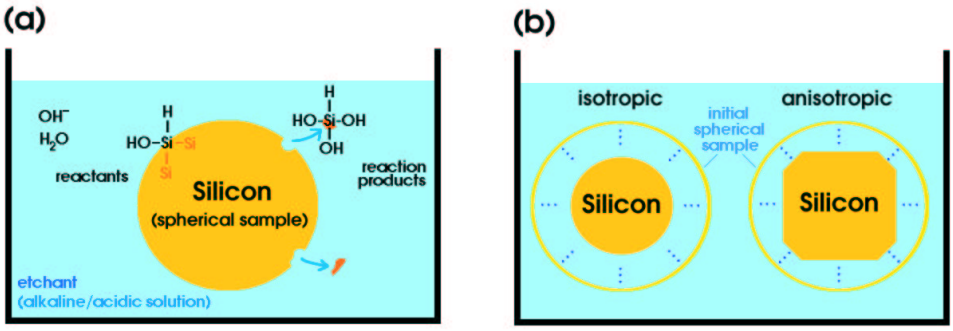

Figure 1: (a) Schematic illustration of the dissolution process during wet etching. (b) Wet etching can be isotropic or anisotropic.

of the crystal usually changes during exposure implies that the etching process is anisotropic, *i.e.* it is faster along certain crystallographic directions than along others (Fig. 1(b)). More properly, the anisotropy of the etching process refers to the orientation dependence of the etch rate, which is defined as the ratio of the distance advanced by the surface to the time of exposure. The anisotropy of the wet etching process is a most valuable property as it provides a low-cost, precise processing technique for the production of three-dimensional micromachined structures with smooth, shiny surfaces. It is mainly this feature that positions wet etching as the most widely used processing technique in silicon technology.

The anisotropy of the wet etching process can be readily determined by the use of a wagon-wheel masking pattern (such as silicon oxide, SiO_2, or silicon nitride, Si_3N_4) on a silicon wafer (Fig. 2(a)). By selectively masking the wafer surface with material that is inert to the action of the etchant the removal of material is forced to occur vertically at the non-masked areas and laterally as the side walls under the masking spokes are uncovered (Fig. 2(b)). Beautiful patterns are formed as a result of the side walls being etched at different rates (Fig. 2(c)). The etch rate of

each side wall orientation (distance r) is obtained from the lateral under-etch rate (distance w) after proper correction by a simple geometrical factor (Fig. 2(b)). Alternative methods to determine the anisotropy of the etching

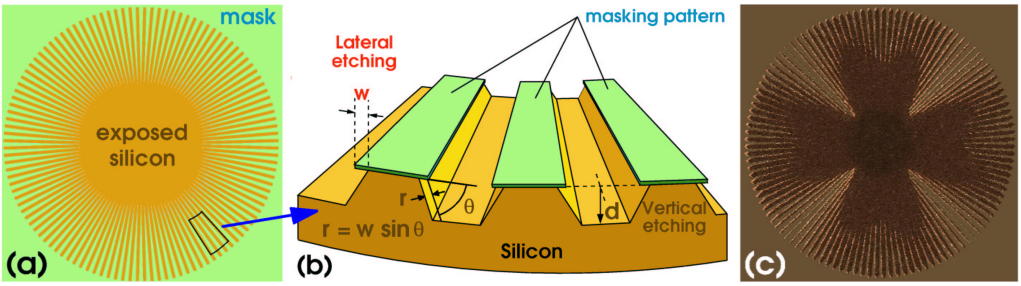

Figure 2: (a) Wagon-wheel masking pattern on silicon before etching. (b) Vertical etching (distance d) and lateral under-etching (distance w). (c) Flower pattern generated during anisotropic etching.

process have been presented in the literature. Examples are the use of wafers with different orientations, a hemispherical crystal [47] or a micromachined wagon-wheel structure without mask [48] (not equivalent to the previous wagon-wheel mask) where $\theta = 90^o$ for all side walls.

The origin of this macroscopic anisotropy in the etching process lies in the site-specificity of the etch rates at the atomistic scale. Since each surface site reacts with the etchant in a different manner and each surface orientation contains a different combination of surface sites, the macroscopic etch rate takes a value that is different for each orientation. Clarifying the origin of this site-specificity is one of the main results of this Thesis. In addition to the number of backbonds exhibited by each surface site (universally accepted as a major source of site-specific etch rates), this Thesis concludes that the site-specificity is determined to a large extent by steric hindrance of OH-termination (Publications II-IV). This result is consistent with the existence of a postulated pentavalent transition state during nucleophilic displacement of H by OH^- [38] and modifies the picture from previous approaches in which the existence of local strain and departure from the tetragonal geometry have been used to explain site-specificity [49]. It is concluded that the structural rigidity of the neighbourhood represents a more accurate measure of reactivity.

In addition to the orientation dependence of the etch rate, also the morphology of the etched surfaces turns out to be orientation dependent when

examined at micrometer and smaller length scales. Representative examples of the features that are typically found on the etched surfaces are pyramidal hillocks, round and triangular pits, zigzag structures and polygonal and straight steps (Figure 3). An important achievement of this Thesis is to

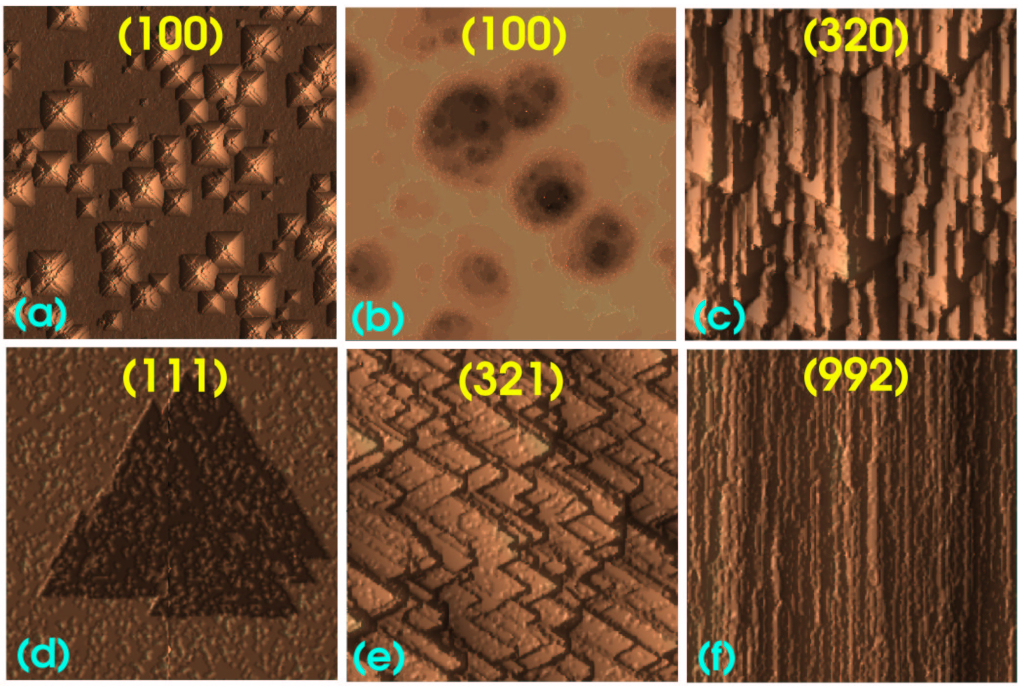

Figure 3: Most frequent (simulated) morphological features during wet chemical etching: (a) Pyramidal hillocks on (100). (b) Round shallow pits on (100). (c) Nosed zigzags on vicinal (110). (d) Triangular pits on (111). (e) Polygonal steps on terraced vicinal (111). (f) Straight steps on terraced vicinal (111). (See Publication V for details.)

show that the same two atomistic processes that explain the existence of site-specific etch rates describe correctly not only the temperature and concentration dependence of the anisotropy (Publications III - V), but also that of the surface morphology (Publication V). This ultimately demonstrates that the macroscopic anisotropy of the etch rate (Figure 2(c)) and the surface morphology of each orientation (Figure 3) are two manifestations of the same microscopic behaviour at different length scales and that a particular realization of one manifestation is uniquely related to a specific realization of the other, as stressed in Figure 4. This is an important observation as it provides two alternative approches for the simulation of the etching process

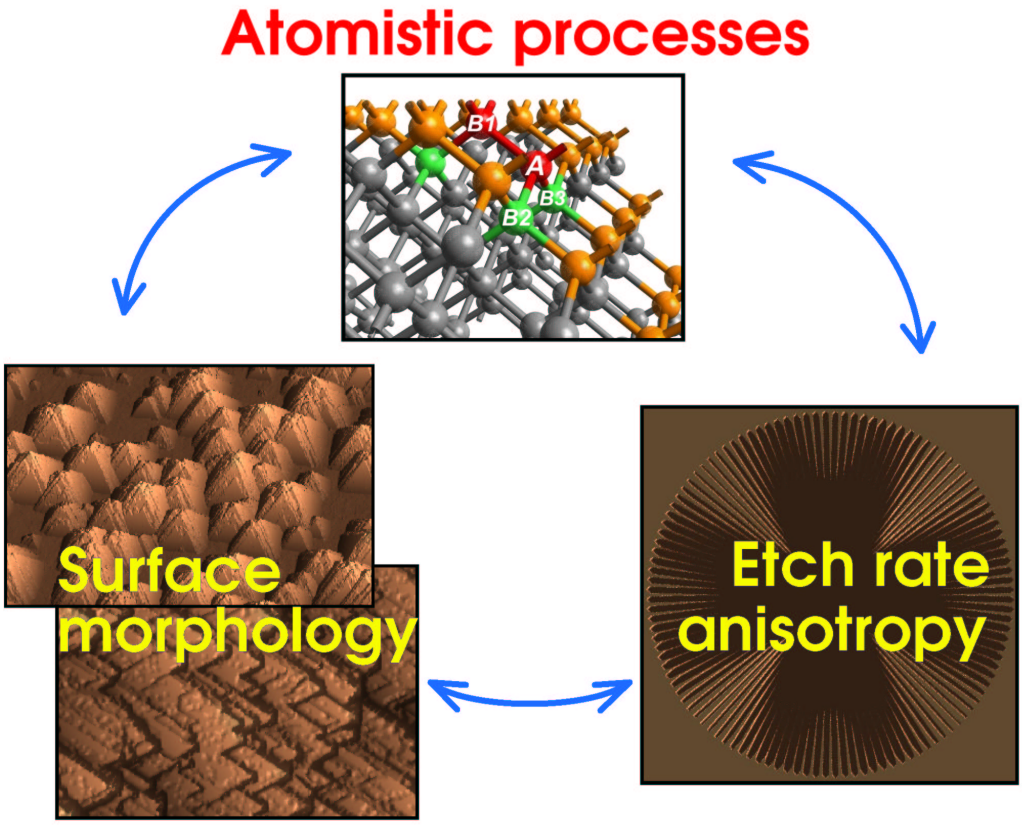

Figure 4: Interrelation between microscopic, mesoscopic and macroscopic features of the etching process.

for device applications. In the first approach, the microscopic parameters of the atomistic model are obtained by fitting the experimental anisotropy of the etch rate and the corresponding intrinsic surface morphology is obtained during the simulations. Alternatively, the microscopic parameters can be obtained by fitting the experimental morphologies and the corresponding intrinsic etching anisotropy can be determined during the simulations. An example of the latter approach is provided in Publication V. This shows that the atomistic model presented in this Thesis can directly serve as a simulation tool for device processing applications.

The anisotropy of the etching process and the quality of the surface finish (the surface morphology) are very sensitive to a long list of parameters. In addition to the choice of bulk + etchant system, the following variables should be controlled during an etching experiment: the etchant concentra-

tion, the temperature, the presence of metal impurities in solution (which depends on water and etchant purity), the use of alcohols (such as IPA) and oxidizing agents as additives in the etch bath, the concentration of silicon in solution, the presence of dissolved oxygen in solution, the use of biasing potentials and stirring, and the level of oxygen impurities in the bulk of the material. Publications III and IV provide a detailed look at the concentration dependence of the etch rate and Publication V considers the effect of this parameter as well as temperature on the surface morphology. Publication VI provides a detailed study of the temperature dependence of the etch rate. In Publication V the important role of the metal impurities for the formation of pyramidal hillocks is considered.

3 Electrochemistry

The removal of surface atoms in wet chemical etching is a complex process that involves chemical and electrochemical reactions [18]. These are distinguished by the fact that the latter involves the participation of free charge carriers, giving rise to measurable currents and allowing for the possibility of controlling the etching process with a biasing potential [17, 21, 40, 41, 42, 43]. As shown in Figure 5, the etching process takes place through sequential oxidation and etching reactions. The chemical and electrochemical reaction routes provide two alternative mechanisms for the oxidation of the hydrogen-terminated sites before the actual removal of the resulting hydroxyl-terminated silicon. The fact that the surface of silicon is predominantly H-terminated during anisotropic etching [31, 38, 49] is explained by recognizing that the oxidation step is the rate limiting process. Once the substitution of H by OH has taken place, a fast sequence of chemical steps (represented as 'etching' in the figure) leads to the removal of the silicon atom (as a $Si(OH)_4$ product). This triggering effect of the OH ligand is attributed to the difference in electronegativities between Si and O, resulting in the polarization and weakening of the backbonds, which, as a result, become more vulnerable to further attack.

The fact that the predominant H-termination is determined by reaction kinetics rather than thermodynamics implies that the site-specificity of the whole process is a result of the rate limiting oxidation reaction alone. From the point of view of simulations, this allows for an important simplification: the etching subprocess can be regarded as infinitely fast and only the oxi-

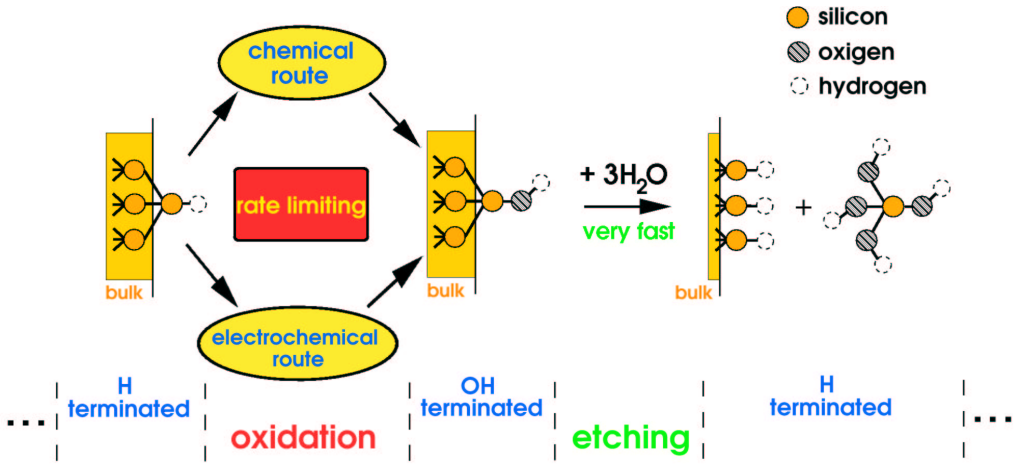

Figure 5: Schematic representation of the oxidation and etching reactions that sequentially occur for the removal of surface atoms. The rate limiting process (oxidation) can take place through chemical and electrochemical routes. Only the nearest underlying bulk atoms in the neighbourhood of the surface site are depicted.

dation subprocess needs to be modelled. This will be the approach in the kinetic Monte Carlo and Cellular Automaton simulations performed in this Thesis.

It should be noticed that, although the hydroxyl group OH plays an important role in catalysing the removal of surface atoms by favoring backbond attack, the active etching species which produces the backbond attack during the etching subprocess is a polar molecule, typically H_2O in alkaline solutions (as indicated in Fig. 5) or, for instance, the HF molecule in a solution containing fluoridric acid. This actually ensures H-termination of the underlying atoms after the etching subprocess. Since the OH-terminated Si surface atom is positively charged with respect to the underlying atoms, the OH group (F) of H_2O (HF) will bond preferentially to the surface atom and the underlying atoms become H-terminated.

3.1 Chemical oxidation

In the oxidation subprocess of Fig. 5, the difference between the chemical and electrochemical routes lies in the mechanism that provides the first hydrogen substitution by a hydroxyl ligand. It is widely accepted that water

molecules and hydroxyl ions OH^- are involved in the chemical oxidation of the H-terminated silicon [17, 21, 41, 49], which also produces hydrogen molecules:

$$\equiv \text{Si–H} + \text{H}_2\text{O} \xrightarrow{\text{OH}^-} \equiv \text{Si–OH} + \text{H}_2 \qquad (1)$$

The hydroxyl ion acts as a catalyst, as depicted in Figure 6, reducing the energy barrier to overcome the formation of a (postulated) pentavalent transition state [38, 49]. It is not clear, however, whether the OH^- ion takes directly part in the reaction, as shown in Fig. 6, or it is the OH group from the water molecule that bonds to the silicon. The fact that both OH^- and

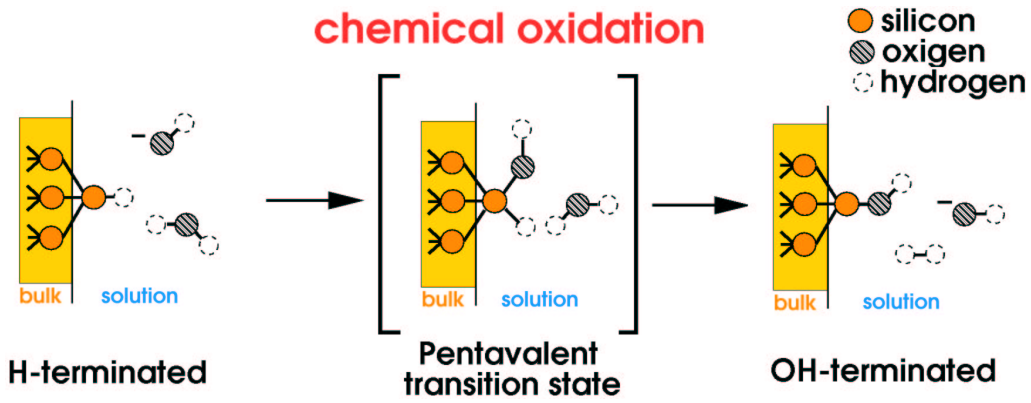

Figure 6: Schematic representation of the chemical oxidation reaction. After [38]. Only the nearest underlying bulk atoms in the neighbourhood of the surface site are shown.

H_2O are involved in the reaction is inferred from the experimental fact that the etching process depends strongly on the concentration of OH^- [32, 34] and it is accompanied by strong evolution of hydrogen bubbles [50]. Actually, anisotropic etching and hydrogen bubbling are so tightly interrelated that the formation of bubbles is frequently used as an indicator of the onset of chemical etching [21, 41]. The ultimate proof for the importance of water and the catalysing action of the OH group (in the oxidation and etching subprocesses) is the fact that etching of crystalline silicon occurs in pure water[1], where a small concentration of OH^- exists, whilst it does not occur in concentrated HF, where the concentration of OH^- is too low to provide the oxidation subprocess depicted in Fig 6. In the case of the latter, the process stops after the H-termination produced by the etching subprocess.

[1] if the temperature is sufficiently high (boiling) and no dissolved oxygen is present in the solution [19, 31, 33, 35].

In view of this reaction mechanism, the site-specificity of the oxidation subprocess (which controls the site-specificity of the whole etching process) can be attributed to one (or all) of the three following possibilities: steric hindrance, local strain and configurational rigidity. Since, according to Fig. 6, it is necessary to have both a water molecule and a hydroxyl ion in the proximity of the site, the amount of empty space around the surface site (steric hindrance) is important for the reactivity. Also, the local strain in the tetrahedral geometry of the site can be used as an indicator of reactivity as the more strained sites should present a lower barrier to the fulfilment of the pentavalent transition state. Finally, the rigidity of the neighbourhood will affect the reactivity. It is not the same to be linked to three rigidly constrained bulk atoms than to three easily deformable atoms in a molecule. Although all three mechanisms are related, each of them stresses a different aspect of the process and, thus, they three should be considered together. Nevertheless, the atomistic model that is presented in this Thesis emphasizes the role of steric hindrance and configurational rigidity, as accounted by the interactions between the surface terminating species. (see Section 4.2 and the 'Discussion' in Publication IV). As a result of these constraints, the chemical oxidation reaction of Fig. 6 is very anisotropic. As an example, it is strongly hindered at (111) terrace sites but it occurs rather easily at kink sites.

3.2 Electrochemical oxidation

Although the previous oxidation reaction is consistent with the dependence of anisotropic etching on pH, the formation of hydrogen bubbles and the site-specificity, it does not account for the existence of measurable currents in electrochemical studies [17, 21, 40, 41, 42]. In fact, the etching process is found to depend on the applied potential. Etching occurs below the passivation potential (corresponding to the peak in anodic current) but it is stopped above that value [41]. Although the details of the electrochemical oxidation are not completely known, the fact that the anodic current is only weakly dependent on the concentration of OH^- [17, 41] suggests that water is the only active species:

$$\equiv \text{Si–H} + \text{H}_2\text{O} \quad \longrightarrow \quad \equiv \text{Si–OH} + 2\text{e}^-_{CB} + 2\text{H}^+ \tag{2}$$

As shown in Figure 7, the process is thought to occur through the dissociation of the ≡Si–H group and subsequent reaction with an H_2O molecule.

The last step involves double electron injection to the conduction band (CB). Note that the electron stays localized at the surface site after dis-

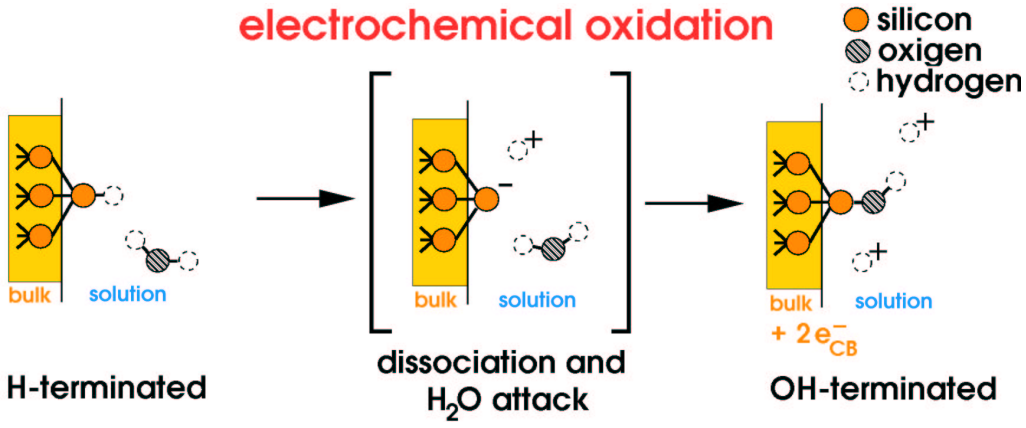

Figure 7: Schematic representation of the electrochemical oxidation reaction. Only the nearest underlying bulk atoms in the neighbourhood of the surface site are shown. After [17].

sociation and that it is only promoted to the conduction band (with a companion electron) during the interaction with the water molecule. It is considered that the use of an anodic potential drives the first electron away from the surface state to the conduction band, favoring the H_2O attack and speeding up the etching process.

Since the dissociation process leaves behind enough space for the reaction with water and the dissociation may occur at any surface site, independently of its configurational rigidity, the electrochemical oxidation is a rather isotropic reaction in comparison to the chemical counterpart, although it implies a higher activation energy due to double injection. As a result, the surface microstructure during wet chemical etching depends on the relative importance of the two oxidation processes. The etching process is most anisotropic for a cathodic bias, where the oxidation is entirely chemical and it becomes increasingly more isotropic as the anodic bias is increased before the passivation value is reached [17]. In this way, flat (111) surfaces without pits can be obtained in conditions where the electrochemical oxidation is sufficiently eliminated. Nevertheless, under usual etching conditions without biasing potentials, the etching process is markedly anisotropic and the electrochemical oxidation route is regarded to have only minor effects (mainly the nucleation of pits on (111)). From the simulational point of

view, the electrochemical reaction is then not taken into account in the atomistic model presented in this Thesis.

Within the previous model, etch stop at the passivation (and higher) anodic potentials [21, 40, 41] is the result of too frequent electrochemical oxidation that leads to increased OH-termination. The interaction between the hydroxyl ligands on the surface produces the formation of silicon oxide through oxygen insertion into the Si–Si backbonds. Since the etching mechanism of SiO_2 is very different from that of silicon, the etching process is stopped. This is the same effect as observed with increasing dissolved oxygen in the solution [35]. In fact, the typical effect of oxygen and other oxidizing agents that are added to the etching solutions is to make the etching process more isotropic [28, 49], improving the surface finish of (100), but negatively affecting that of (111), just in the same manner as the biasing potentials.

It should be noticed that a rather different model for the complete etching process has been presented in Ref. [41] in which the oxidation subprocess is considered as a chemical process and it is the etching subprocess that presents alternative chemical and electrochemical routes, depending on the conditions. This model, however, will lead to complete OH-termination under weak anodic bias and in the presence of oxidizing agents and, therefore, to etch stop by silicon oxide formation.

4 Simulating anisotropic etching

4.1 Alternative methods

A number of different strategies for the simulation of anisotropic wet chemical etching have been presented in the literature and two major methods can be identified: the geometrical and the atomistic approaches. In the geometrical simulators the crystal is reduced to a finite set of crystallographic planes for which the etch rates are known. The surface of the crystal is approximated by a set of facets corresponding to these planes, and the time evolution is discretized. Within each time step, each plane forming a part of the surface evolves along its normal direction, experiencing a displacement according to the known etch rate for that particular plane. The change in geometry at the intersecting lines between adjacent crystallographic planes or at the edge of a masked region is determined using the Wulff-Jaccodine

method [51, 52]. In the ideal case, these simulators require the knowledge of complete etch rate diagrams, to be obtained experimentally [53, 54]. The more complete the etch rate diagram is, the more accurate the geometrical etch simulator will become. However, since only a finite set of etch rates can be accessed experimentally, this approach presents difficulties to describe curved non-crystallographic geometries and corrugated surface finish from experiments. Besides, the fact that new crystal faces can emerge at vertices and edges multiplies the number of possibilities that have to be considered by the three-dimensional implementations and performance becomes slow. In spite of these difficulties, a number of 3D etch simulators have been reported [55, 56].

The second family of anisotropic etch simulators is based on an atomistic approach. The crystal is described at a more microscopic level as a collection of cells (or, as in this Thesis, atoms). The neighbourhood of an atom at the surface directly affects the probability with which the etchant can break its backbonds to the rest of the structure and the atom is removed or remains attached accordingly. Due to the randomness involved in the removal of atoms, the evolving crystal surface shows roughness at various scales, in agreement with experiments. Hybrid approaches combining both geometrical and atomistic models have been reported [57, 58].

Within the atomistic approach it is possible to distinguish between Cellular Automaton (CA) and Monte Carlo (MC) schemes. The two simulation methods differ in the way how the time evolution of the crystal surface is handled, enphasizing different aspects of the etching process. In the CA approach, the surface is updated as a whole, after each atom has been visited and a decision has been taken with respect to its removal (parallel update). In the MC scheme, the surface is updated sequentially, right after each decision is taken (sequential update). As a result, the CA scheme enphasizes the evolution of the system as a whole entity whilst the MC method stresses the importance of each individual process. The CA approach is well suited for the description of the macroscopic evolution of the process, such as the formation of facetted surfaces at the convex corners of masked samples. However, the MC scheme provides a better tool for the exploration of the surface morphology. In this Thesis, both the MC and CA simulation schemes are considered. By using both methods, information is gained on the mechanisms involved in the complicated process of dissolution and the macroscopic and mesoscopic surface evolution, including the surface morphology and the etch rate. The actual MC and CA schemes used in this

Thesis are presented in Section 4.3 after the atomistic model for the etching process is presented in Section 4.2.

4.2 Atomistic model

Anisotropic wet chemical etching is a non-equilibrium process in which both the microscopic morphology and the macroscopic orientation-dependent etch rate are determined by the relative values of the microscopic (atomistic) reaction rates. In this Thesis it is shown that the origin of the differences in site-specific rates is found in two microscopic mechanisms (Publications II–IV): the weakening of backbonds following OH termination of surface atoms and the existence of significant interaction between the terminating species (H/OH). The weakening of the backbonds depends only on the *total number* of hydroxyls attached to the two atoms sharing the bond and is independent of the particular distribution of the OH groups between the two atoms (Publication II). The energy of a bond between an atom terminated by i OH groups and an atom terminated by j groups ($i, j = 0, 1, 2, 3$) can be written as

$$\epsilon_{ij} = \epsilon_o - (i + j) \cdot \epsilon \quad , \tag{3}$$

where $\epsilon_o \approx 2.7$ eV is the bond energy between two bulk atoms and $\epsilon \approx 0.4$ eV is the energy reduction for every OH group that is attached to either atom. Correspondingly, the total bonding energy for a surface atom with n first neighbours is simply the sum of the energies of the n bonds:

$$E_{\text{bonds}} = \sum_{j=1}^{n} \epsilon_{m,m_j} \quad , \tag{4}$$

where the most general case has been considered in which the target atom is terminated by m OH groups ($m \leqslant 4 - n$) and the j-th first neighbour ($j = 1, 2, .., n$), having itself n_j first neighbours, is terminated by m_j OH groups ($m_j \leqslant 4 - n_j$).

The other microscopic mechanism of major importance in wet chemical etching, namely, the interaction between the surface terminating groups (H/OH), occurs only in the presence of *indirect second neighbours* (Publications III–IV). These are next-nearest neighbours which cannot be reached from the target atom (TA) by a covalent-bond path passing directly through a first neighbour (FN), in opposition to the *direct* second neighbours which

are linked to the TA by a covalent path *directly* passing through a FN. As an example, the second neighbours C1 through C6 in Figure 8(a) are *direct* whilst the second neighbours C7 and C8 are *indirect*. The presence of an

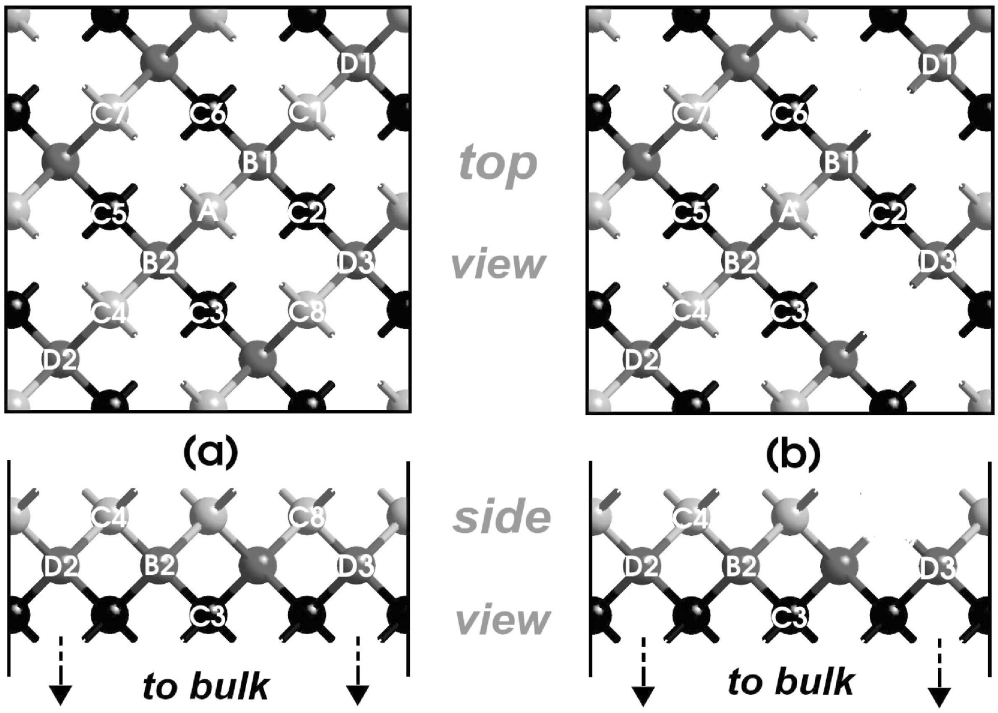

Figure 8: (a) A typical atom (A) in an ideal (100) surface having 2 first neighbours (B1-B2) and 8 second neighbours (C1-C8). C1 through C6 are examples of *direct* second neighbours and, C7 and C8, of *indirect* second neighbours. (b) Atom A has now only 6 second neighbours (C2-C7). Note that D1 restricts the attachment of a hydroxyl onto B1 in the same manner as C7 does for A. Atoms are shaded lighter at the surface and become darker towards the bulk.

indirect second neighbour imposes additional geometrical restrictions to hydroxyl termination of the target atom due to the extra interaction between the hydroxyl group and the terminating species (H or OH) attached to the indirect neighbour. As shown in Figure 8(b), similar restrictions can also occur for the attachment of hydroxyl groups to the *first neighbours* of the target atom. Note that the termination state of the first neighbours has major implications for the value of the bonding energy of the target atom (Equation 4) and, thus, the restrictions in OH-attachment at the *first neigh-*

bours become relevant. Due to these interactions, hydroxyl termination of the target atom (and its first neighbours) involves additional energy terms, not taken into account in Eq. (4). As a result, the total (local) energy of a surface atom can be expressed as the sum of three terms (Publication III):

$$E = E_{\text{bonds}} + \sum(e^{TA}_{OH/H} + e^{TA}_{OH/OH}) + \sum(e^{FN}_{OH/H} + e^{FN}_{OH/OH}) \ , \qquad (5)$$

where E_{bonds} is the energy of Eq. (4) and $\sum(e^{TA}_{OH/H} + e^{TA}_{OH/OH})$ ($\sum(e^{FN}_{OH/H} + e^{FN}_{OH/OH})$) symbolically denotes the total energy from the interactions between the OH groups terminating the TA (FN) and H and/or OH terminating the indirect second neighbours of the TA (FN). The geometrical restrictions to hydroxyl termination in the presence of indirect second neighbours is a manifestation of the important role of steric hindrance in anisotropic wet chemical etching. In the present model, the source of steric hindrance is identified as the (H/OH-terminated) indirect second neighbours.

Note that, although the parameters ϵ and ϵ_o used for describing the bonding energy are fixed by the first-principles *ab-initio* study (Publication II), the interaction energies $e^{TA,FN}_{OH/OH}$ and $e^{TA,FN}_{OH/H}$ can be used as tunable parameters in order to describe different etchants. Once an etchant is chosen, its concentration is described in the model by the amount of surface coverage by OH-groups (Publication III). Fig. 9 shows the expected qualitative dependence of the surface coverage θ as a function of the concentration of OH ions in solution. Note that the amount of OH coverage saturates for

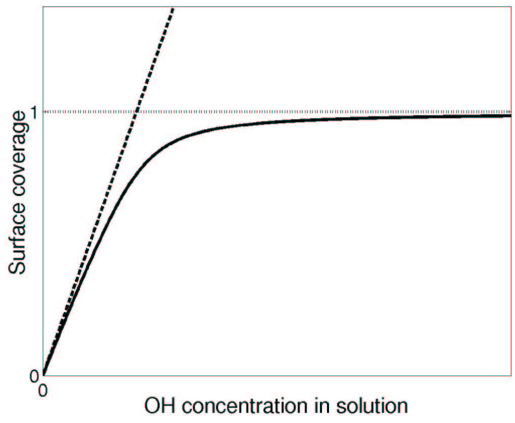

Figure 9: Qualitative dependence of the surface coverage θ with respect to the concentration of OH ions.

sufficiently large concentrations, since the reaction kinetics at the surface is overwhelmed by the amount of OH ions available. On the other hand, for low enough concentrations, the coverage should increase linearly, because the average distance between OH ions (or OH clusters, if these are formed) attached at the surface is large enough, making it possible for new attachments to occur in between existing ones without any extra interaction. In the intermediate region, no local maxima should be expected, because it would imply the existence of a parabolic minimum in the dissolution of the reaction products as a function of concentration, whilst only a parabolic maximum can be expected in this case. Therefore, the linear behaviour changes monotonically to saturation.

The dynamics of the surface consists of random removals of surface atoms with probabilities:

$$p_\alpha = p_{0\alpha} \mathrm{e}^{-\Delta \mathrm{E}_\alpha / \mathrm{k_B T}}, \tag{6}$$

where the activation energy ΔE_α is defined as:

$$\Delta E_\alpha = max(0, E - E_\alpha). \tag{7}$$

Here, $p_{0\alpha}$ and E_α are parameters describing the different surface atom types ($\alpha = 1, 2A, 2B, 2C, 3A, 3B$). Note that the local energy E is calculated using the same expression (Eq. 5) for all site types independently of the value of α. The function $max(0, E - E_\alpha)$ is used to conform with the Metropolis algorithm [59]. Following the notation used in surface studies of Si(111) (*e.g.* [44, 49]), the following surface site types are considered (Figure 10):

- Type **3A**: Three-bonded atoms at ideal (111) surfaces: *terrace monohydrides* (TM, atom A in Figure 10(a)).
- Type **3B**: Three-bonded atoms at ideal $[1\overline{2}1]$ steps: *step monohydrides* (SM, atom A in Figure 10(b)); plus all other possible three-bonded atoms.
- Type **2A**: Two-bonded atoms on ideal (100) surfaces: *terrace dihydrides* (TD, atom A in Figure 10(d)).
- Type **2B**: Vertical two-bonded atoms at ideal $[\overline{1}2\overline{1}]$ steps: *vertical step dihydrides* (VSD, atom A in Figure 10(c)).
- Type **2C**: Horizontal two-bonded atoms at ideal $[\overline{1}2\overline{1}]$ steps: *horizontal step dihydrides* (HSD, atom B in Figure 10(c), when the A atoms have been removed); plus all other possible two-bonded atoms.

- Type **1**: Singly-bonded atoms: *trihydrides* (TRI); also referred to as *kinks*.
- Type **0**: Non-bonded atoms that have not been removed: *unlinked* (UL)

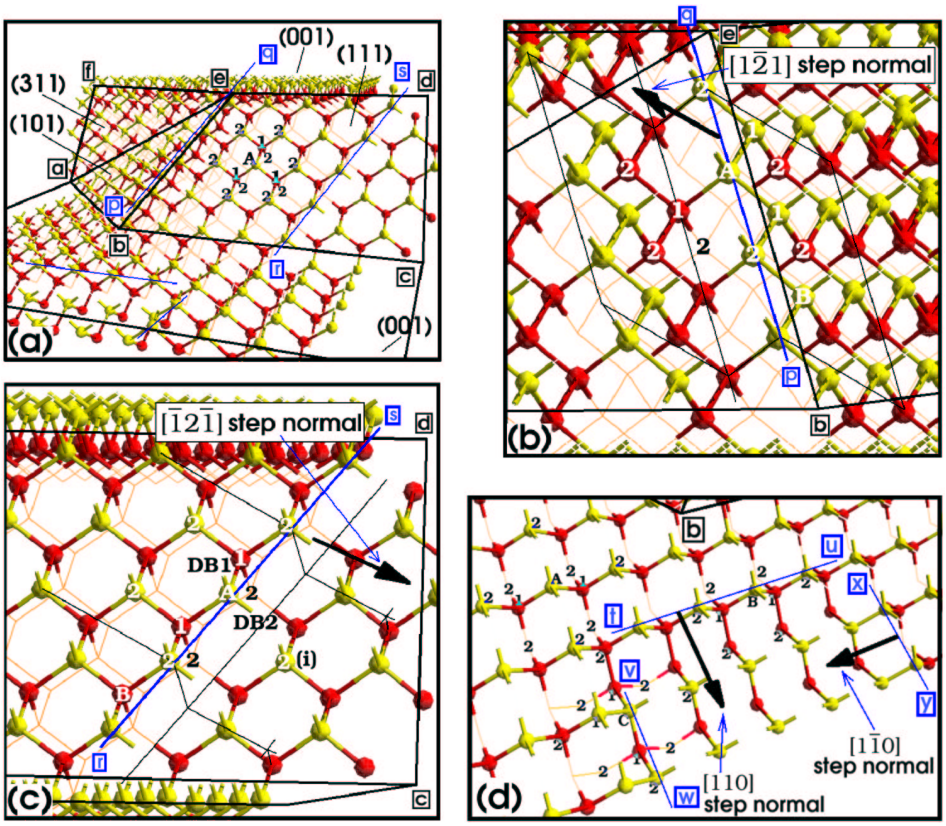

Figure 10: (a) Half of the symmetrical structure appearing at an under-etched convex corner at low coverage θ (Publication III). Closer views are shown from arbitrary directions for: (b) a $[1\bar{2}1]$ step, (c) a $[\bar{1}2\bar{1}]$ step and (d) the (001) plane with several $\langle 110 \rangle$ steps. Surface atoms are yellow (shaded lighter) and backbonded atoms red (darker). Steps are characterized by the direction of their normal. First and second neighbours are labelled as **1** and **2**, respectively. Indirect second neighbours are marked with **(i)**. Boxed letters are used to ease comparison between (a)-(d).

Note that the atoms of type **0** are included for completeness since they can occasionally appear in connection to the formation of overhangs. This is,

however, a rare event in the simulations and has no measurable effect on the evolution of the surface. These atoms are removed (with probability one) as soon as they are encountered and, accordingly, the surface contains $M = 6(+1)$ types of atoms in this model. Note also that due to the different possible combinations of the terminating species H and OH around a surface site, the activation energies $\Delta E_\alpha = E - E_\alpha$ will take different values even for the case of atoms of the same type α.

The six pairs of parameters $(p_{0\alpha}, E_\alpha)$ for Types **1**, **2A**,...**3B** can be determined from comparison to experiment. The idea is to choose the parameters so that the relative values of the etch rates of a number of surface orientations (six, in principle) agree with those from an experiment. By adjusting the parameters p_0, the simulated etch rates will shift up/down in an Arrhenius plot. Similarly the slopes of the etch rates can be controlled by tuning the parameters E_c. Alternatively, it is also possible to choose the parameters $(p_{0\alpha}, E_\alpha)$ based on comparison of the simulated surface morphology with that from experiments. An example of this approach is provided in Publication V.

The macroscopic evolution of the surface is obtained using either a Kinetic Monte-Carlo or a Cellular Automaton scheme, which randomly chooses surface sites and decides whether they are removed or not according to the probabilities p_i. More details about these methods are given in the following Section.

4.3 Monte Carlo and Cellular Automaton simulation schemes

In the atomistic simulations of anisotropic etching the atoms of the surface are visited one by one and their neighbourhoods are inspected in order to determine the probability of removal and to decide whether the atom is removed or remains attached. The probability of removal is related to the state of the neighbourhood because it determines not only the number of backbonds (which need to be broken in order to remove the atom) but also their energy (Section 4.2). Usually, the criterion used in these models in order to remove the surface atoms is simple: removal occurs if a random number is smaller than the removal probability corresponding to the current configuration of the neighbourhood (Eq. 5); otherwise, the surface atom remains attached.

Figure 11 shows the flow diagrams corresponding to the Monte Carlo and Cellular Automaton schemes. In both cases, the simulation is carried out by discretizing the time evolution in time steps (counter t) until the final time $t = T$ is reached.

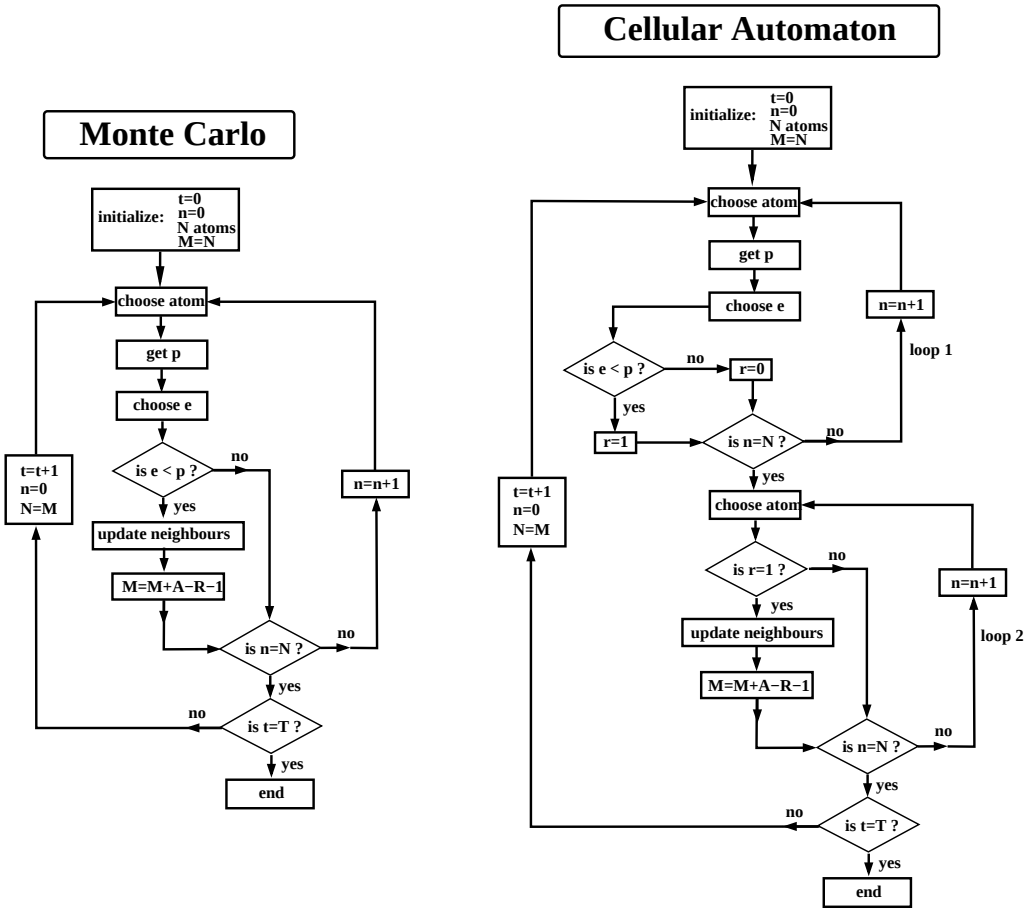

Figure 11: Flow diagrams for the Monte Carlo and Cellular Automaton schemes.

In the MC scheme, for each time step t a loop of local update iterations is carried out (counter n). The maximum value attainable by n (i.e. N, the length of the time step) is the number of surface atoms found at the beginning of the time step ($n = 0$). Each local update iteration occurs at a randomly chosen atom from the current surface. Once the value of the removal probability p has been determined (according to Eq. 5), a random number e is chosen in order to decide whether the atom will leave or stay.

In the event that $e \leq p$, the chosen atom is removed but otherwise a new local update iteration will be started. If the chosen atom is removed, the state of the neighbourhood is updated and the number of atoms at the surface is modified as $M = M + A - R - 1$, where A is the number of first neighbours which were in the bulk before the removal of the atom (as they are added now to the surface) and R is the number of first neighbours that are removed as a consequence of being bonded only to the atom that has left, which itself is counted as -1. If the number of local update iterations n is already equal to the size of the surface at the beginning of the MC time step (N), then a new time step ($t = t + 1$) is initiated ($n = 0$) which will include $N = M$ local update trials. Otherwise, a new local update is tried ($n = n + 1$). If the number of MC time steps is already equal to T the program finishes.

In the CA scheme, two loops are carried out within one time step t. In the first loop, the removal of each surface atom is decided according to the previous removal criterion. The atoms that are removed are marked with $r = 1$ and the ones that stay with $r = 0$. In the second loop, all those surface atoms for which removal has been decided ($r = 1$) are removed and the state of their neighbourhoods and the size of the surface are updated as explained for the MC scheme. The time evolution of the whole surface is obtained as these complete surface updates are consecutively generated ($t = t + 1$) until the final value T is reached.

Note that the CA scheme enphasizes the evolution of the surface as a complete entity whilst the MC method stresses the importance of each individual microscopic process. As a result, the CA can be used for the description of macroscopic features of the process, such as e.g. the formation of facetted surfaces at the convex corners of masked samples (see Publication III), but it is not so well suited for the exploration of the surface morphology. This is, however, the ideal scenario for the MC scheme (see Publication V). Both methods provide useful determinations of the macroscopic etch rate (see Publications III-VI).

The algorithms shown in Fig. 11 are probably the simplest approach for both methods, pedagogically easy to present but not necessarily efficient from a computational point of view. In both cases, if the removal probability p is very low, most of the computational time will be spent generating random numbers e, as the most frequent output from the removal criterion will be 'no'. A solution to this potential inefficiency is to 'choose' always a successful event and to increment time according to the inverse of the

removal probability [60]. Note that the measure of time in the MC and CA simulations as the number of iterations in the shown algorithms is proportional to real time. This is ultimately demonstrated by the results obtained on the time evolution of the process features (see Publications III and V).

5 Overview of results

5.1 Anisotropy

As explained in Section 2, the anisotropy of the wet etching process can be readily determined by the use of a wagon-wheel masking pattern on a silicon wafer. It should be noticed that the use of such a mask causes the apparition of all possible microscopic configurations of an atom at any of the (hkl) surfaces enforced by the <hk0>-aligned masking spokes. This mask is thus a difficult test for any model trying to explain the etching mechanism. By comparing the experimental pattern with those simulated with and without interactions between the surface terminating species, Figure 12 shows that the anisotropy of the etching process is explained by the proposed atomistic mechanisms. Note that the features at regions Q and R are not predicted when the interaction between the terminating species is not considered (Fig. 12(b)). The correct prediction of the fastest-etched planes (region Q) is controlled by the incorporation of the indirect second neighbours in the simulation (Fig. 12(c)). This shows that such an important macroscopic feature of the etching process as the location of the fastest-etched planes is actually due to the steric hindrance imposed by the indirect second neighbours on the termination probability by hydroxyl groups.

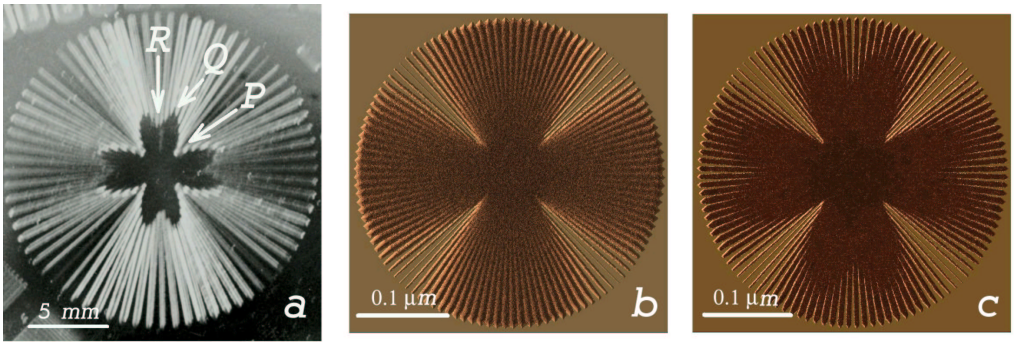

Figure 12: Comparison between (a) experiment (Publication I), (b) simulation using only the 'backbond-weakening' mechanism and (c) simulation incorporating the additional steric hindrance by indirect second neighbours. The details of these simulations are given in Publication II.

5.2 Morphology

In the same way as the macroscopic anisotropy of the etching process is explained by the proposed atomistic model, also the rich orientation-dependent surface morphology associated to the process is shown to have its origin at the atomistic scale. As an example, Figure 13 shows the simultaneous formation of shallow round pits on (100) (Fig. 13(a)), nosed zigzag structures on vicinal (110) (Fig. 13(b)-(c)), straight (Fig. 13(d)) and polygonal (Fig. 13(e)) steps on vicinal (111) and triangular etch pits on exact (111). Similar behaviour is obtained when pyramidal hillocks are observed on (100), as Figures 3(a),(c)-(f) show. The details of all these simulations and the corresponding analysis of the characteristic atomistic processes that control these different morphologies are given in Publication V.

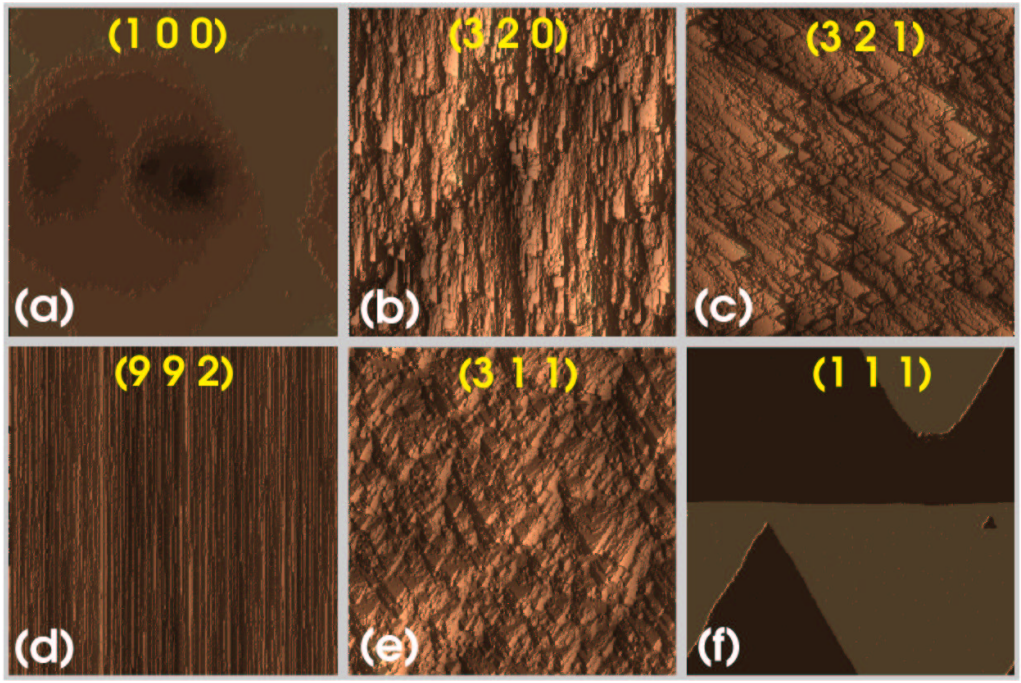

Figure 13: Characteristic morphologies observed at representative orientations when shallow round pits are the characteristic feature on (100). All simulations are done with the same parameters. Compare to Fig. 3(a),(c)-(f).

5.3 Time evolution

The microscopic model also reproduces the time evolution of the surface morphology. As an example, the typical behaviour observed in the undercutting process occurring at the convex corners of masking patterns is presented at the right-hand-side column of Fig. 14. In addition, the time

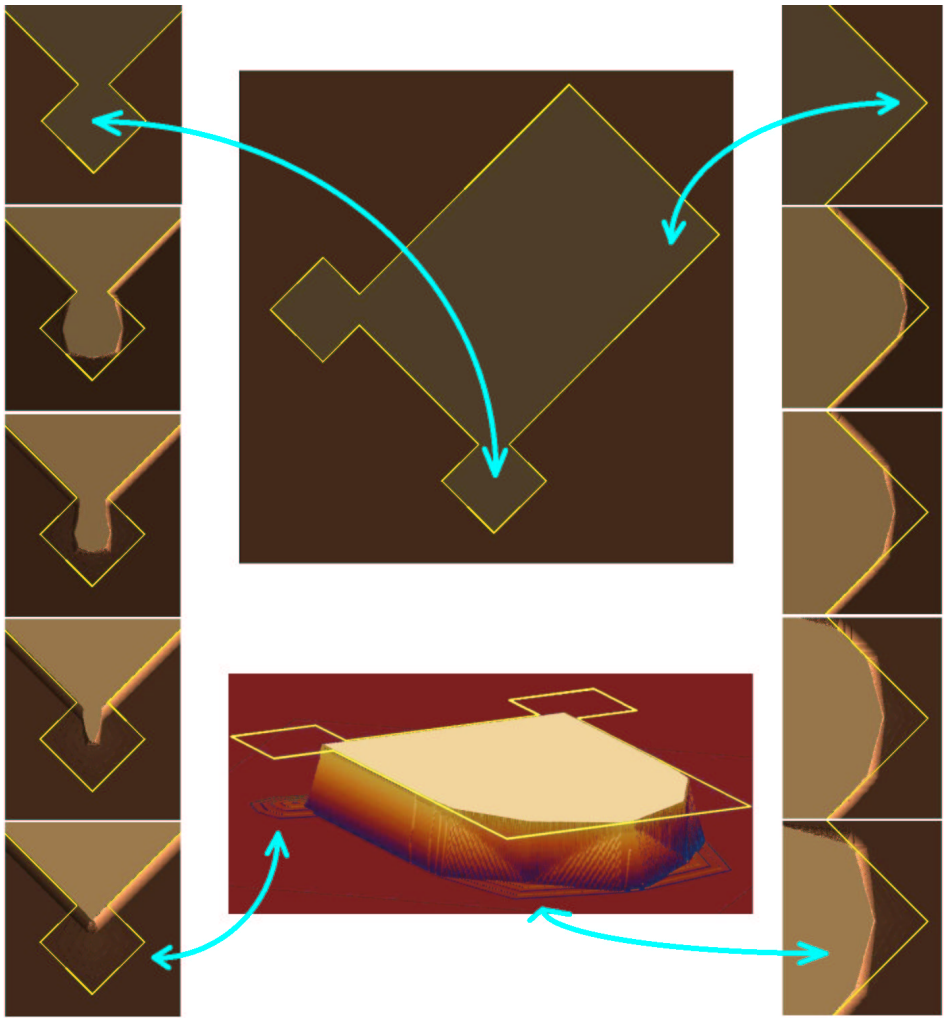

Figure 14: Time evolution of the etching process around convex corners. The planar size of the systems in the central column is 0.23 μm $\times$ 0.23 μm.

evolution for a typical convex-corner compensating structure is shown on

the left-hand-side column of the figure. As in the experiments, the compensating structure provides the elimination of undercutting. The microscopic model predicts that after a certain time/depth, the corner will present the desired 90 degree form (as seen from the top). The details about this simulation are given in Publication III.

Similarly, Figure 15(a)-(f) shows the typical time evolution of the (100)-surface morphology, which is characterized initially by the nucleation and growth of pyramidal hillocks, and by a complete surface texturization by the hillocks for long etching times. Note that, at any time, pyramids of different sizes are observed, reflecting the fact that hillocks are nucleated continuously during the etching process. The nucleation mechanism of the hillocks is considered in detail in Publication V.

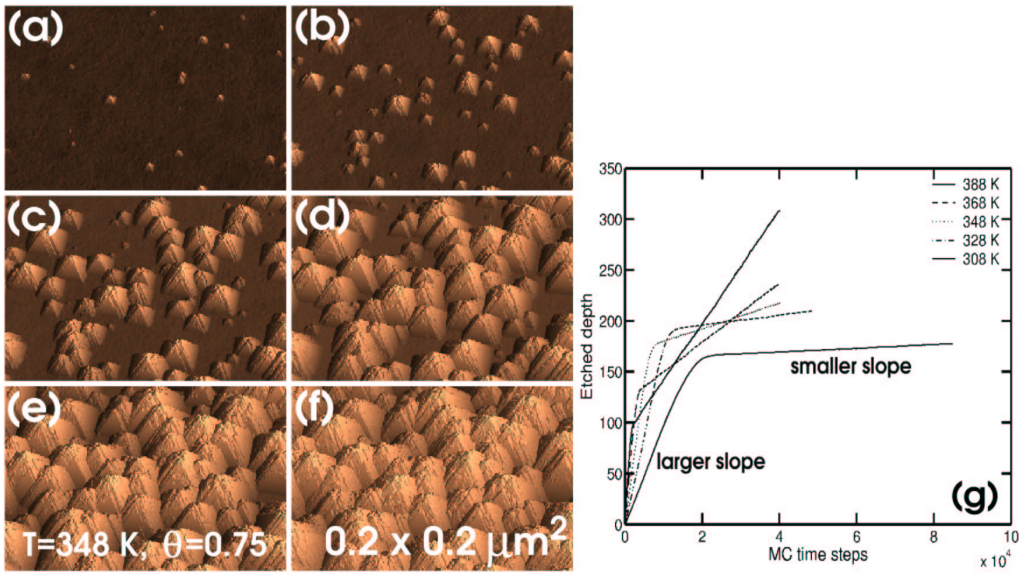

Figure 15: (a)-(f) Surface texturization of Si(100) as time evolves. (g) Time dependence of the etched depth in the simulation shown in (a)-(f) (T=348 K) and for four additional temperatures.

The eventual complete surface texturization by hillocks has a dramatic effect on the value of the macroscopic etch rate. As shown in Figure 15(g), the etch rate experiences a large change as a function of time. As a result, the usual determination of the etch rate as the ratio of the total etched depth to the total time becomes an ill-defined quantity unless the surface is monitored to detect the onset of complete texturization and, thus, the

division between the two etch rate regimes. This issue is considered in more detail in Publication V.

From a general perspective, the results of this Thesis confirm that the macroscopic evolution of an etched surface, including its motion, roughness and morphology, reaches a well-defined steady state independent of the initial state and the particular details of the transient period. Actually, it is the fact that a steady-state exists for each surface orientation that allows the study of the surface morphology and the activation energy in Publications V and VI, respectively.

5.4 Concentration dependence

The proposed atomistic model can be used to study the effect of changes in the concentration of the etchant by varying the amount of OH-coverage θ. As an example, Figure 16 shows how the anisotropy of the etching process increases with θ for the particular conditions in those simulations (Publication III). This behaviour has important consequences on the shapes

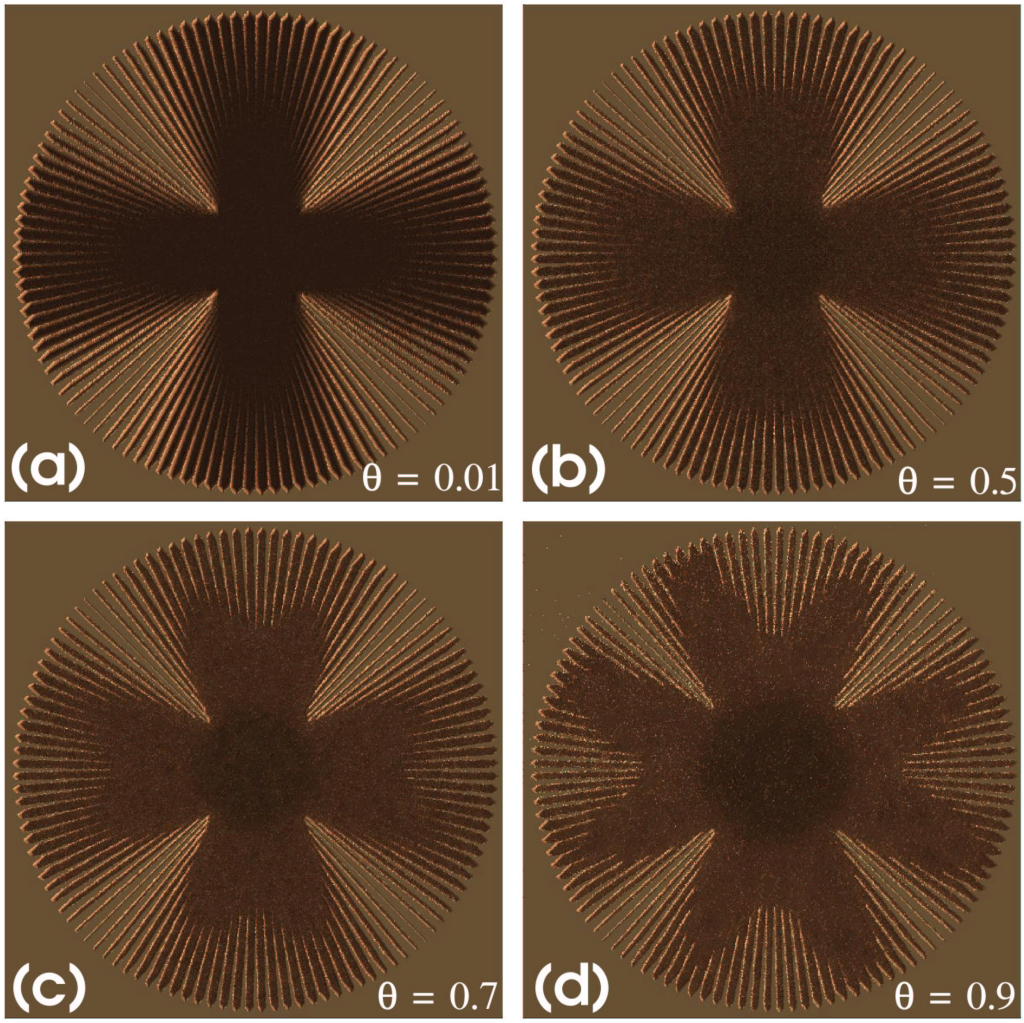

Figure 16: Etching of Si(100) wafers masked with a wagon wheel pattern for different OH coverage values: (a) $\theta = 0.01$, (b) $\theta = 0.5$, (c) $\theta = 0.7$, and (d) $\theta = 0.9$. The planar size of the systems is 0.35×0.35 μm^2. $T = 348$ K.

of the under-etched convex corners, as shown in Figure 17, and on the surface morphology, as shown in Figure 18. These various manifestations of the dependence of the etching process on coverage are due to the fact that the competition between backbond weakening (favouring removal) and steric hindrance (preventing it) takes place in a rather particular way at each surface site. Changing θ, the relative site-specificity of the reaction rates will be altered. A more detailed discussion of these effects is given in Publications III, IV and V.

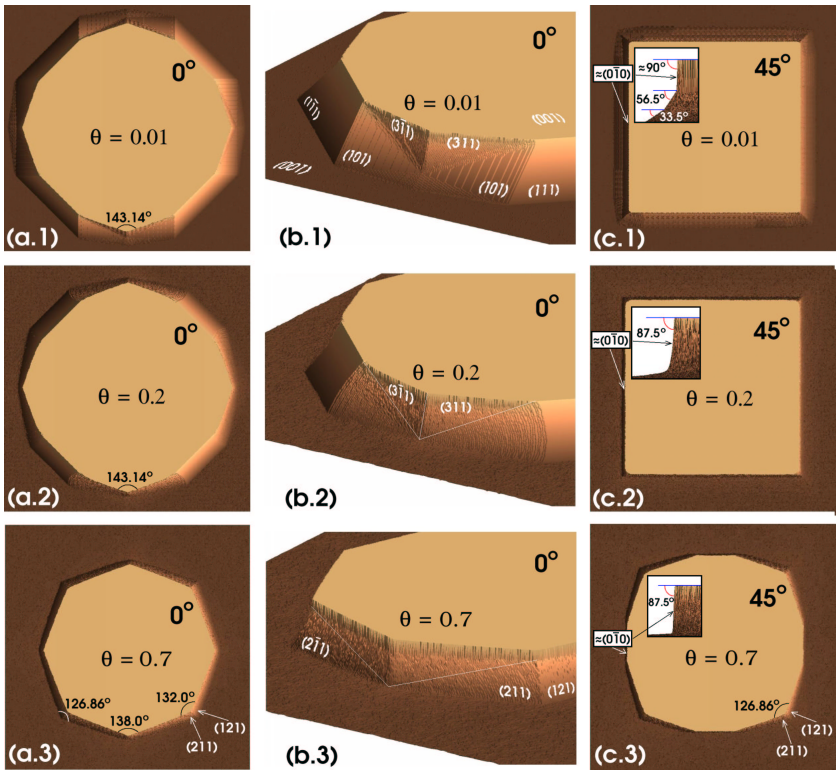

Figure 17: Surface morphology and under-etching at convex corners of square-shaped masks oriented making an angle $\alpha = 0^o$ (columns (a) and (b)) and $\alpha = 45^o$ (column (c)) with the $\langle 110 \rangle$ direction on a Si(001)-oriented crystal. Results for three different coverage values $\theta = 0.01$ (row 1), $\theta = 0.2$ (row 2) and $\theta = 0.7$ (row 3) are shown. Each snapshot in column (b) is a close-up detail of the lower corner of each of the snapshots in column (a). The inserts in column (c) show the under-etched profiles along the sides. The planar size of the systems is 0.23×0.23 μm^2. The etched depth is 18 nm in all cases. $T = 348$ K.

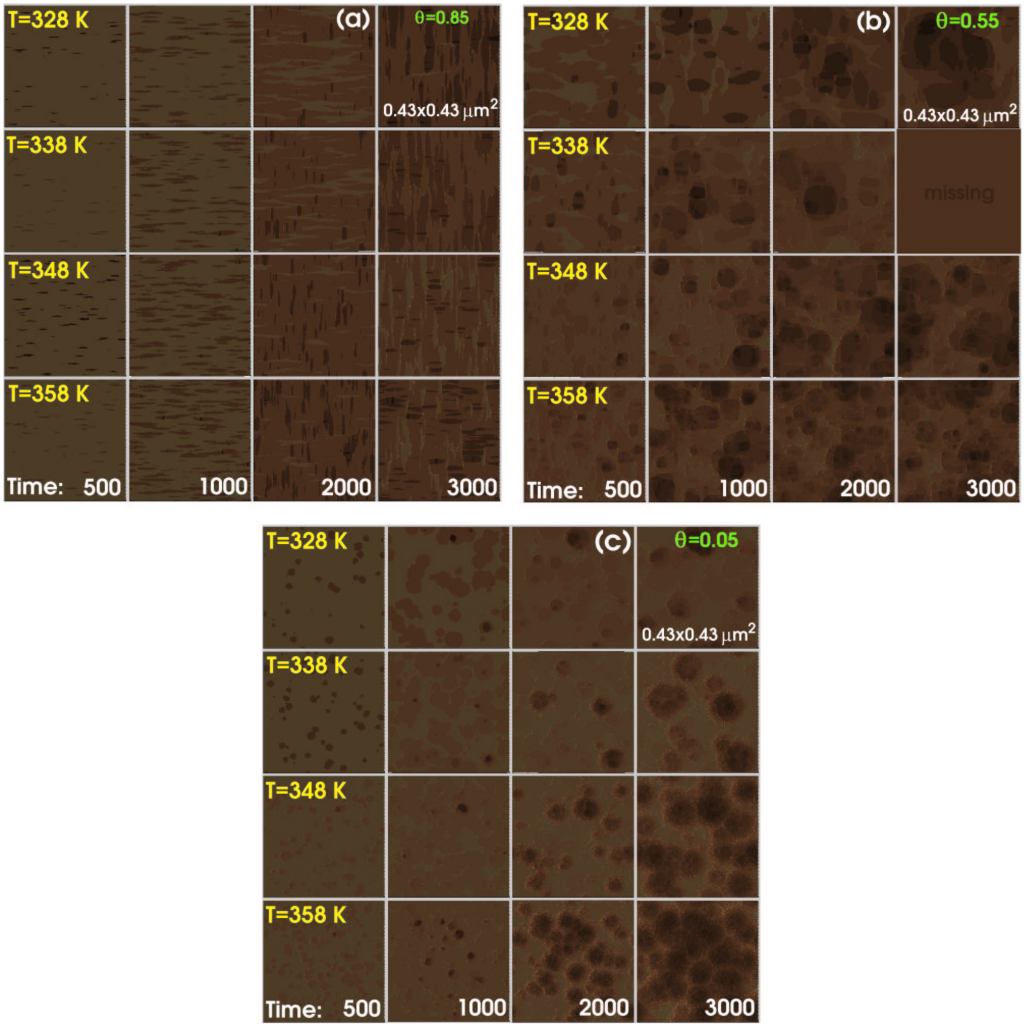

Figure 18: Dependence of the morphology of (100) on the coverage (θ) by OH groups. for conditions preventing the formation of pyramidal hillocks.

5.5 Temperature dependence, activation energy

Also the temperature dependence of the etching process can be studied by the use of the atomistic model. As an example, the exponential increase in the density of pyramidal hillocks on Si(100) with temperature (Figure 19) is explained in Publication VI as a result of the competition between the disclosure of weakly bonded surface atoms (favouring the formation of more hillocks) and the removal of impurity atoms (which destabilizes them).

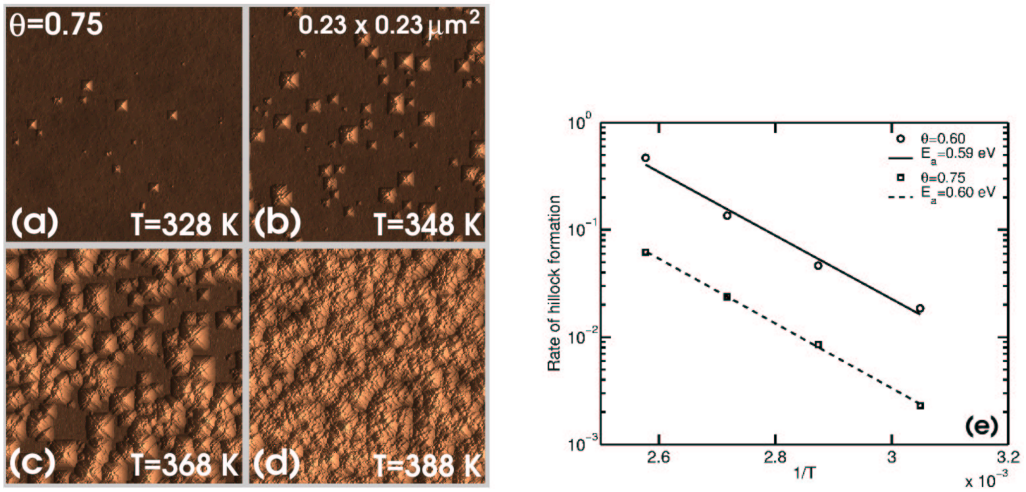

Figure 19: (a)-(d) Temperature dependence of the density of hillocks. (e) Arrhenius dependence of the number of hillocks for two different OH-coverage values.

An important application of the possibility to vary the temperature in the model is the study of the macroscopic activation energy of the etch rate. The determination of the apparent macroscopic activation energy which, roughly speaking, corresponds to the slope of the straight lines in an Arrhenius plot (Figure 20), is a trivial task if data is available at different temperatures. However, its interpretation is not always so clear. Although it is common practice to refer to it as a complicated weighted average over the activation energies of the atomistic processes involved, the lack of an explicit relation has frequently lead to its interpretation as the activation energy of the rate-limiting process. This is probably due to the fact that this process is related to the removal of the majority species on the surface, so that an (erroneous) association is done by assigning the largest weight for the average to this species.

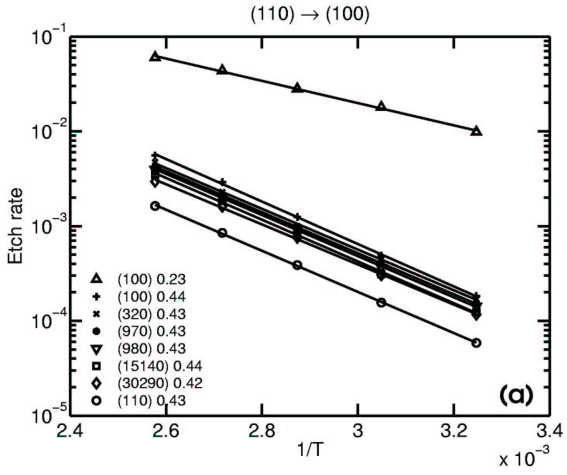

Figure 20: Arrhenius behaviour of the etch rates of planes (100), (110) and vicinal (110). The higher (lower) data for (100) corresponds to the etch rate before (after) surface texturization.

The problem of unveiling the relation between the microscopic and macroscopic activation energies, and the determination of the relative weight of each different microscopic process is solved in Publication VI. The conclusion is that the macroscopic activation energy E_a is the sum of two terms $E_a = E_a^{(p)} + E_a^{(f)}$ (Figure 21(a)). The first term $E_a^{(p)} = \sum_\alpha \langle w_\alpha^\uparrow \rangle E_{\langle p_\alpha \rangle}$ - sometimes wrongly identified as the activation energy itself - corresponds to the average of the microscopic activation energies $E_{\langle p_\alpha \rangle}$ of the (average) removal probabilities $\langle p_\alpha \rangle$. The additional term $E_a^{(f)} = \sum_\alpha \langle w_\alpha^\uparrow \rangle E_{\langle f_\alpha \rangle}$ accounts for the existence of fluctuations in the surface fractions of particles f_α at fixed temperature. Fig. 21(b) shows that the weights $\langle w_\alpha^\uparrow \rangle$, defined as the normalized fractions of removed particles

$$\langle w_\alpha^\uparrow \rangle = \langle f_\alpha \rangle \langle p_\alpha \rangle / \sum_\beta \langle f_\beta \rangle \langle p_\beta \rangle \ , \tag{8}$$

are good approximations for the relative contributions ϵ_α of each atom type to the total macroscopic activation energy,

$$\epsilon_\alpha = \langle w_\alpha^\uparrow \rangle \left(E_{\langle f_\alpha \rangle} + E_{\langle p_\alpha \rangle} \right) / \sum_\beta \langle w_\beta^\uparrow \rangle \left(E_{\langle f_\beta \rangle} + E_{\langle p_\beta \rangle} \right) \ . \tag{9}$$

This allows for the unambiguous identification of the particular surface species which effectively control the process, even if the actual values of $E_{\langle f_\alpha \rangle}$ and $E_{\langle p_\alpha \rangle}$ (required to evaluate ϵ_α) are not known *a priori*.

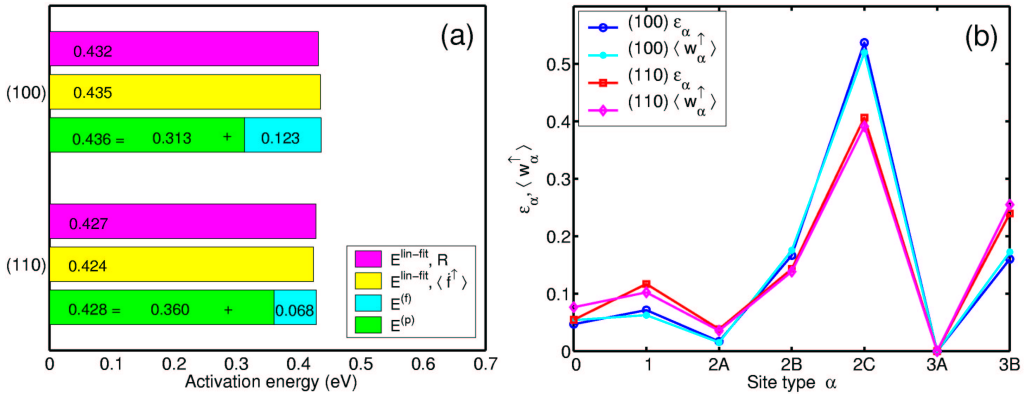

Figure 21: (a) Macroscopic activation energies of (100) and (110) explained as the sum of two terms $E_a = E_a^{(p)} + E_a^{(f)}$. (b) Relative contributions of each surface site ($\alpha = 1, 2A, 2B, ...$) to the macroscopic activation energy of (100) and (110). Exact measures (ϵ_α) and their approximations ($\langle w_\alpha^\uparrow \rangle$) are given. See Publication VI for more details.

6 Summary of Publications

6.1 Publication I

The need to consider the second neighbours in order to describe the anisotropy of the etching process is demonstrated. This is done by directly comparing the macroscopic anisotropy of the simulated systems with that of experiments, as implied by the formation of flower patterns in wagon-wheel masked wafers and under-etching behaviour. A microscopic removal probability function is presented as a way to parameterize the large differences in the reaction rates of the different surface sites (i.e. the site-specificity) instead of using one parameter (the removal probability) for each site. The removal probability function can be considered as a manner to account for steric hindrance, although the origin itself of the geometrical restrictions will not be understood until Publication II.

From a computational point of view, the essential form of the kinetic Monte Carlo (KMC) program that is used throughout this Thesis is described in detail in this Publication. It includes a description of the system initialization process in the presence of masks and a brief account on the surface visualization method. No major changes have been required in the processing part of the program (the KMC scheme), except for some small variations to accomodate the way how the removal probabilities are determined in succesive versions of the atomistic model. The only major upgrade in the program is the incorporation of the possibility to simulate the etching process for any crystallographic orientation. By just specifying the (hkl) Miller indeces of the surface, large systems (nearly at the micrometer scale) with or without masks can be routinely simulated.

6.2 Publication II

The double role of the next nearest neighbours in anisotropic etching is clarified by introducing a distinction between direct and indirect second neighbours (DSN and ISN, respectively). The combination of first-principles calculations and kinetic Monte Carlo simulations shows that the macroscopic anisotropy of the etching process is explained by two atomistic mechanisms: the weakening of the backbonds following OH termination of surface sites, a process that depends on the presence or absence of DSNs, and the steric

hindrance for OH-termination in the presence of ISNs. This explains why it was necessary for the removal probability function used with success in Publication I to depend explicitly on the total number of second neighbours.

6.3 Publication III

The method for consideration of the second neighbours is completed in this Publication. An important subtle feature, namely, the fact that the indirect second neighbours of the first neighbours need to be taken into account, is demonstrated. This completes the search for an atomistic model that describes the essential features of anisotropic etching.

This Publication shows the large potential of the model for the description and understanding of the etching process and its applications. As an example, the long-standing fundamental question of why the etch rate is a non-monotonic function of the concentration of OH^- in solution (with a maximum at an intermediate pH value) is explained as a trade-off between the weakening of backbonds and the interactions between the surface-terminating hydroxyls. The predictive power of the atomistic model, including the correct time evolution, is demonstrated by performing simulations of under-etching at different OH-coverages. This shows that the etching process should not be considered as a macroscopic process involving the optimization of an evolving facetted surface (the geometrical simulator approach of Section 4.1), but rather as an atomistic process leading to the formation of curved bounding surfaces displaying a corrugated morphology. An important result of this paper is the fact that etch pitting and step propagation at any orientation can be understood as different manifestations of the two microscopic processes considered in the atomistic model presented.

6.4 Publication IV

This Publication presents concisely but with a more general perspective the atomistic model conceptualized during Publications I-III. An explanation for the dependence of the relative stability of step monohydrides and dihydrides on the etchant concentration is given within the framework of the atomistic model. This explains the formation of triangular or hexagonal pits on Si(111), depending on the concentration and the nature of the etchant. Based on the performance of the atomistic model, which takes into account

structural rigidity through steric hindrance, the use of structural rigidity as an indicator of site reactivity is concluded to be more suitable than that of local strain.

6.5 Publication V

This Publication demonstrates that the surface morphology can be understood as another manifestation of the two atomistic processes that describe the macroscopic anisotropy. It is shown that (metal) impurities in solution have an important role in the nucleation, growth and evolution of pyramidal hillocks on Si(100) surfaces, although it is acknowledged that oxide micromasks and/or re-growth of silicon can occasionally provide the necessary nucleation mechanism and that hydrogen bubbles have also an important role, providing an effective amplifying mechanism. The fact that the temperature dependence of the density of hillocks follows an Arrhenius behaviour and decreases with increasing concentration are explained. Also, the formation of shallow round pits on Si(100) and their dependence on concentration are explained. It is demonstrated that the nucleating mechanisms of morphologically related structures such as pyramidal hillocks on Si(100) and nosed zigzags on vicinal Si(110) is not necessarily the same, modifying the standard accepted picture. The simulations confirm that the formation of (one-layer-deep) triangular pits on exact Si(111), and of polygonal (saw-shaped) and straight steps between the terraces in vicinal Si(111) is controlled by the relative rate of $[1\overline{2}1]$ and $[\overline{1}2\overline{1}]$ step-propagation and depends on the misorientation of the surface with respect to Si(111).

6.6 Publication VI

This Publication considers the relation between microscopic and macroscopic activation energies and, as such, it can be considered as a culmination of the ultimate purpose of this Thesis, namely, the stablishment of the interrelation between the features of the etching process at the different length scales. The use of Monte-Carlo simulations shows that the apparent macroscopic activation energy is only partially explained by the expected expression for the average over the microscopic activation energies and that an additional term accounting for the existence of fluctuations in the fractions of particles has to be taken into account. The results obtained are

very general and applicable to non-equilibrium surface processing such as surface cleaning and growth.

References

[1] C. Merveille, Sensors and Actuators A **60**, 244–248 (1997).

[2] A. Hein, S. Finkbeiner, J. Marek, and E. Obermeier, *Proc. SPIE* vol. **3876** pp. 29–36 (1999).

[3] J. D. Johnson, S. R. Zarabadi, J. C. Christenson, and Tracy A. Noll, *SAE technical papers* **2002-01-1080**.

[4] L. Qiu, A. Hein, E. Obermeier, and A. Schubert, Sensors and Actuators A **54**, 547–551 (1996).

[5] J. Garra, S. Brida, L. Ferrario, and M. Paranjape, Sensors and Materials **13**(6), 351–358 (2001).

[6] S-J. Paik and D-I. Cho, *Proc. of the 3rd Workshop on Physical Chemistry of Wet Etching of Silicon*, ed. K. Sato, Nara, Japan (2002) pp. 68–73.

[7] N. Nozawa, K. Kakushima, G. Hashiguchi, and H. Fujita, *Proc. of the 3rd Workshop on Physical Chemistry of Wet Etching of Silicon*, ed. K. Sato, Nara, Japan (2002) pp. 52–53.

[8] T. Gessner, W. Dötzel, D. Billep, R. Hahn, C. Kaufmann, S. Kurth, K. Kehr, C. Steiniger, and U. Wollmann, *Proc. SPIE* vol. **3008** pp. 296–305 (1997).

[9] M. Sasaki, T. Fujii, and K. Hane, *Proc. of the 3rd Workshop on Physical Chemistry of Wet Etching of Silicon*, ed. K. Sato, Nara, Japan (2002) pp. 54–57.

[10] M. Hoffmann, P. Kopka, T. Gross, and E. Voges, J. Micromech. Microeng. **9**, 151–155 (1999).

[11] A. J. Nijdam, E. van Keuren, and M. Paranjape, *Proc. of the 3rd Workshop on Physical Chemistry of Wet Etching of Silicon*, ed. K. Sato, Nara, Japan (2002) pp. 47–51.

[12] S-S. Tan, M. Reed, H. Han, and R. Boudreau, J. Microelectromech. Syst. **5**(1), 66–72 (1996).

[13] H. J. Cho, K. W. Oh, C. H. Ahn, P. Boolchand, and T-C. Nam, *IEEE Transactions on Magnetics* **37**(4), 2749–2751 (2001).

[14] J. Knoch, J. Appenzeller, B. Lengeler, R. Martel, P. Solomon, Ph. Avouris, Ch. Dieker, Y. Lu, K. L. Wang, J. Scholvin, and J. A. del Alamo, J. Vac. Sci. Technol. A **19**(4), 1737–1741 (2000).

[15] G. J. Pietsch, U. Köhler, and M. Henzler, J. Appl. Phys. **73**(10), 4797–4807 (1993).

[16] P. Allongue, V. Costa-Kieling, and H. Gerischer, J. Electrochem. Soc. **140**(4), 1009–1018 (1993).

[17] P. Allongue, V. Kieling, and H. Gerischer, Electrochim. Acta **40**, 1353–1360 (1995).

[18] P. Allongue, Phys. Rev. Lett. **77**(10), 1986–1989 (1996).

[19] K. Arima, K. Endo, T. Kataoka, Y. Oshikane, H. Inoue, and Y. Mori, Surf. Sci. **446**, 128–136 (2000).

[20] L. M. Landsberger, S. Naseh, M. Kahrizi, and M. Paranjape, J. Microelectromech. Syst. **5**(2), 106–116 (1996).

[21] X. H. Xia and J. J. Kelly, Electrochimica Acta **45**, 4645–4653 (2000).

[22] P. K. Singh, R. Kumar, M. Lal, S. N. Singh, and B. K. Das, Solar Energy Materials and Solar Cells **70**, 103–113 (2001).

[23] A. J. Nijdam, E. van Veenendaal, H. M. Cuppen, J. van Suchtelen, M. L. Reed, J. G. E. Gardeniers, W. J. P. van Enckevort, E. Vlieg, and M. Elwenspoek, J. Appl. Phys. **89**(7), 4113–4123 (2001).

[24] P. Allongue, C. H. de Villeneuve, S. Morin, R. Boukherroub, and D. D. M. Wayner, Electrochimica Acta **45**, 4591–4598 (2000).

[25] P. Raisch, W. Haiss, R.J. Nichols, and D.J. Schiffrin, Electrochimica Acta **45**, 4635–4643 (2000).

[26] M. L. Munford, R. Cortès, and P. Allongue, Sensors and Materials **13**, 259–269 (2001).

[27] T. A. Newton, Y-C. Huang, L. A. Lepak, and M. A. Hines, J. Chem. Phys. **111**, 9125–9128 (1999).

[28] S. P. Garcia, H. Bao, M. Manimaran, and M. A. Hines, J. Phys. Chem. B **106**, 8258–8264 (2002).

[29] X. Zhou, M. Ishida, A. Imanishi, and Y. Nakato, Electromchimica Acta **45**, 4655–4662 (2000).

[30] H. J. Lewerenz, H. Jungblut, and S. Rauscher, Electrochimica Acta **45**, 4615–4627 (2000).

[31] G. S. Higashi, Y. J. Chabal, G. W. Trucks, and K. Raghavachari, Appl. Phys. Lett. **56**, 656–658 (1990).

[32] P. Jakob and Y. J. Chabal, J. Chem. Phys. **95**(4), 2897–2909 (1991).

[33] S. Watanabe, K. Horiuchi, and T. Ito, Jpn. J. Appl. Phys. **32**, 3420–3425 (1993).

[34] G. J. Pietsch, G. S. Higashi, and Y. J. Chabal, Appl. Phys. Lett. **64**, 3115–3117 (1994).

[35] S. Watanabe and Y. Sugita, Appl. Surf. Sci. **107**, 90–94 (1996).

[36] S. Watanabe, Appl. Surf. Sci. **130–132**, 231–236 (1998).

[37] P. A. Thiry Y. Caudano and Y. J. Chabal, Surf. Sci. **502–503**, 91–95 (2002).

[38] M. A. Hines, Y. J. Chabal, T. D. Harris, and A. L. Harris, J. Chem. Phys. **101**(9), 8055–8072 (1994).

[39] N. Miyata, S. Watanabe, and S. Okamura, Appl. Surf. Sci. **117–118**, 26–31 (1997).

[40] P. Allongue, V. Costa-Kieling, and H. Gerischer, J. Electrochem. Soc. **140**(4), 1018–1026 (1993).

[41] P. M. M. C. Bressers, S. A. S. P. Pagano, and J. J. Kelly, J. Electroanal. Chem. **391**,159–168 (1995).

[42] W. Haiss, P. Raisch, D. J. Schiffrin, L. Bitsch, and R. J. Nichols, Faraday Discuss. **121**, 167–180 (2002).

[43] O. Tabata, Sensors and Materials **13**, 271 – 283 (2001).

[44] J. Kasparian, M. Elwenspoek, and P. Allongue, Surface Science **388**, 50–62 (1997)..

[45] J. Flidr, Y-C. Huang, T. A. Newton, and M. A. Hines, J. Chem. Phys. **108**(13), 5542–5553 (1998).

[46] J. Flidr, Y-C. Huang, and M. A. Hines, J. Chem. Phys. **111**(15), 6970–6981 (1999).

[47] M. Shikida, K. Sato, K. Tokoro, and D. Uchikawa, Sensors and Actuators A **80**, 179–188 (2000).

[48] R. A. Wind, H. Jones, M. J. Little, and M. A. Hines, J. Phys. chem. B **106**, 1557–1569 (2002).

[49] M. A. Hines, Ann. Rev. Phys. Chem. **54**, 29–56 (2003).

[50] H. Schröder, E. Obermeier, and A. Steckenborn, J. Micromech. Microeng. **9**, 139–145 (1999).

[51] R. J. Jaccodine, J. of Appl. Phys. **33**, 2643–2647 (1962).

[52] D. W. Shaw, J. of Crystal Growth **47**, 509–517 (1979).

[53] K. Sato, M. Shikida, Y. Matsushima, T. Yamashiro, K. Asaumi, Y. Iriye, and M. Yamamoto, Sensors and Actuators A **64**, 87–93 (1998).

[54] K. Sato, M. Shikida, T. Yamashiro, K. Asaumi, Y. Iriye, and M. Yamamoto, Sensors and Actuators A **73**, 131–137 (1999).

[55] C. H. Sequin, Sensors and Actuators A **34**, 225–241 (1992).

[56] K. Asaumi, Y. Iriye, and K. Sato, *Proc. of IEEE Micro Electro Mechanical Systems (MEMS'97)* Nagoya, Japan (1997) pp. 412–417

[57] M. Chahoud, A. Schlachetzki and H-H. Wehmann, Sensors and Actuators A **63**, 141–146 (1997).

[58] T. J. Hubbard and E. K. Antonsson, *Proc. of 1996 ASME Design Engineering Technical Conference and Computers in Engineering*, Irvine, California (1996) **96-DETC/DFM-1312**

[59] N. Metropolis, A. W. Rosenbluth, M. N. Rosenbluth, A. H. Teller, and E. Teller, J. Chem. Phys. **21**, 1087–1091 (1953).

[60] H. Camon, Z. Moktadir, Sensors and Actuators **A 46-47** 27-29 (1995)